INTERNATIONAL JOURNAL FOR NUMERICAL METHODS IN FLUIDS
Int. J. Numer. Meth. Fluids 2006; **52**:1059–1092
Published online 10 May 2006 in Wiley InterScience (www.interscience.wiley.com). DOI: 10.1002/fld.1216

A conservative 2D model of inundation flow with solute transport over dry bed

J. Murillo, P. García-Navarro*,†, J. Burguete and P. Brufau

Fluid Mechanics, CPS, University of Zaragoza, Spain

SUMMARY

In this paper, a transient 2D coupled vertically averaged flow/transport model is presented. The model deals with all kind of bed geometries and guarantees global conservation and positive values of both water level and solute concentration in the transient solution. The model is based on an upwind finite volume method, using Roe's approximate Riemann solver. A specific modification of the Riemann solver is proposed to overcome the generation of negative values of depth and concentration, that can appear as a consequence of existing wetting/drying and solute advance fronts over variable bed levels, or by the generation of new ones when dry areas appear. The numerical stability constraints of the explicit model are stated incorporating the influence of the flow velocity, the bed variations and the possible appearance of dry cells. Faced to the important restriction that this new stability condition can impose on the time step size, a different strategy to allow stability using a maximum time step, and in consequence a minimum computational cost is presented. Copyright © 2006 John Wiley & Sons, Ltd.

KEY WORDS: finite volume; upwind method; conservative solution; wetting/drying front; dry bed; stability condition; river flow; solute transport; bounded concentration

INTRODUCTION

Many engineering and environmental problems involve the study of unsteady water flows with solute transport. River flows, in particular, are mostly unsteady and, as they are characterized by the presence of a vertical scale much smaller than the horizontal one, they can be described by the shallow-water model [1] which forms a set of nonlinear hyperbolic equations. The prediction of unsteady flows in a river is important because of the huge impacts on property, human life and environment. A great deal of work has been devoted to develop 1D and 2D numerical models for unsteady shallow flows in the last decades and various

*Correspondence to: P. García-Navarro, Fluid Mechanics, CPS, University of Zaragoza, Spain.
†E-mail: pigar@unizar.es

Contract/grant sponsor: Spanish Ministry of Science and Technology
Contract/grant sponsor: European Research project IMPACT

Received 17 November 2005
Revised 3 February 2006
Accepted 5 February 2006

computational techniques using finite difference, finite element and finite volume methods have been reported [1–6]. Several numerical difficulties must be adequately treated to obtain an accurate solution without numerical errors. Zhao *et al.* [7] provided a good historic revision and the features required for a two-dimensional river flow simulation model: it should be able to handle complex topography, dry bed advancing fronts, wetting–drying moving boundaries, high roughness values, steady or unsteady flow and subcritical or supercritical conditions.

Among the numerical techniques reported, those belonging to the category of conservative methods have gained acceptance in recent years for their important property of providing a proper discrete representation of the physical conservation laws. Essentially imported from gas dynamics, they have been extended to shallow-water problems trying to overcome the relevant differences existing between these two applications. Natural topographies is the main challenge. This involves positive and negative bed slopes that can be steep in many places rendering dominant the bed slope source terms. Dominant source terms and open boundaries are two important difficulties to face when using a conservative method since they both can damage the conservative character of the solution. This topic is addressed in this paper in direct connection with the stability limits of the model. In realistic problems of transient water flow, variable bed levels are always linked to inundation over dry areas.

Wet/dry and dry/wet interfaces between interior cells have traditionally represented a difficulty for modellers wanting to solve the shallow-water equations over a bed of irregular geometry. Flow over dry bed involves a complicated situation that can be analysed as a boundary condition which is dynamically changing in time with the moving front and continuously expanding or reducing the flow domain. Akanbi and Katopodes [8] gave a brief summary of problems encountered in the numerical simulation of flood waves propagating over dry bed. The alternative is to include the wet/dry interfaces in the full domain of computation in which there may be wet cells and dry cells at the same time. In this case, the numerical scheme chosen for the discretization must be able to cope with them. In general, cells being flooded or dried during the computation tend to introduce numerical instabilities in the solution, resulting for example in negative water depths or unphysical high velocities. Different approaches have been proposed to handle them. These techniques include modified equations in very shallow regions [9], shock capturing schemes [10] or the assumption that a cell is dry if water depth is below a small critical value [11]. Beffa and Connel [12] reported numerical oscillations when cells switch from dry to wet or vice-versa. George and Stripling [13] represented the local bathymetry in each cell by a sloping facet rather than by a flat bed to eliminate the spurious shocks in their finite volume model. Some authors working with finite elements solve the problem by allowing the controlled use of negative depths [14–16]. Bradford and Sanders [17] used Neumann extrapolation of the velocity in partially wet cells to bypass the incorrect estimation of pressure and body forces in such cells. In Brufau *et al.* [18, 19], driven by the interest of controlling numerical stability and global mass conservation, a two-dimensional model was presented for unsteady flow simulation where the main strategy was based on a local redefinition of the bed slope at specific locations.

In this paper, a coupled shallow flow/transport two-dimensional finite volume model is formulated exclusively from the point of view of the in-going contributions to the cells of the domain. From the analysis of the waves involved in the upwind finite volume scheme, the time step restriction or stability region is studied in the linear homogeneous case and

a general rule valid for structured and unstructured grids is provided. When source terms are present in the equations, both the flux of information exchanged across the cell edge and the final state at the neighbour cells depend on them. This leads to a redefinition of the stability condition that must be a function not only of the eigenvalues of the problem but also of the source terms themselves. The modification of the stability region of different numerical schemes in a linear approach has previously been stated [20]. It has been proved that noncentred discretization of the source term enlarges the stability region. Furthermore, when not only source terms are important but also dry/wet interfaces appear in the simulation domain, the stability condition becomes even more restrictive. In order to be able to use the largest time step possible, compatible with stability and volume conservation, a modification of the model, equivalent to the local redefinition of the bed slopes, is presented. The new model is conservative, ensures bounded values of concentration in all situations and avoids negative water depths, for both existing and generated wetting/drying advance fronts when new dry areas appear. Despite the notable difference in the size of the allowed time steps, no difference in the numerical solutions appears, as several numerical examples demonstrate.

A first test case of circular dam break flow is used to analyse the properties on the numerical solution for the concentration in exacting conditions. This example shows that the concentration can become unrealistically unbounded as a consequence of the conservative formulation and that the correction proposed in the model is good to control those situations. A second test case of still water with concentration surrounding a prism emerging from water is presented to show the convenience of applying the suggested numerical treatment at the wet/dry limits and the influence of this part of the solution over the concentration values. A test case of unsteady oscillatory flow in a parabolic vessel with analytical solution has been used to validate the unsteady model. An initial concentration has been added to this test case in order to validate the coupled solution in absence of diffusion. Finally, an example of unsteady flow over dry bed with solute transport in a river reach physical model is included as application of the proposed simulation model.

GOVERNING EQUATIONS

The two-dimensional shallow-water equations, which represent mass and momentum conservation in a plane, can be obtained by depth averaging the Navier–Stokes equations. Neglecting diffusion of momentum due to viscosity and turbulence, wind effects and the Coriolis term, they form a system of equations [21]. In the context of a depth-averaged model, the depth-averaged concentration is of primary interest, and it has been shown that, under special conditions, an advection–dispersion model [22] can be defined. Traditionally, both models have been solved independently in a sequential form, solving first the shallow-water equations and next, in function of those flow values, the solute flow equation. In order to improve the accuracy and conservation properties of the solution, both models are coupled in a single system of equations [23], that becomes:

$$\frac{\partial \mathbf{U}}{\partial t} + \frac{\partial \mathbf{F}(\mathbf{U})}{\partial x} + \frac{\partial \mathbf{G}(\mathbf{U})}{\partial y} = \mathbf{S}(x, y, \mathbf{U}) \tag{1}$$

where

$$\mathbf{U} = (h, q_x, q_y, h\phi)^{\mathrm{T}}$$

$$\mathbf{F} = \left(q_x, \frac{q_x^2}{h} + \frac{gh^2}{2}, \frac{q_x q_y}{h}, h\phi u\right)^{\mathrm{T}}, \quad \mathbf{G} = \left(q_y, \frac{q_x q_y}{h}, \frac{q_y^2}{h} + \frac{gh^2}{2}, h\phi v\right)^{\mathrm{T}} \tag{2}$$

$$\mathbf{S} = (0, gh(S_{ox} - S_{fx}), gh(S_{oy} - S_{fy}), \vec{\nabla}(\mathbf{K}h\vec{\nabla}\phi))^{\mathrm{T}}$$

where h represents the water depth, $q_x = uh$ and $q_y = vh$, with (u, v) the depth-averaged components of the velocity vector $\mathbf{u}$ along the x and y coordinates, respectively, ϕ represents the depth-averaged concentration, g is the acceleration of the gravity, S_{ox} and S_{oy} are the bed slopes along the x and y coordinates, respectively, S_{fx} and S_{fy} are the friction losses along the x and y coordinates, respectively, and $\mathbf{K}$ is the empirical diffusion matrix.

The source term vector is split in three different parts treated separately: bottom variations $\mathbf{B}$, diffusion term $\mathbf{D}$, and friction term $\mathbf{R}$: $\mathbf{S} = \mathbf{B} + \mathbf{D} + \mathbf{R}$.

$$\mathbf{B} = (0, ghS_{ox}, ghS_{oy}, 0)^{\mathrm{T}}$$

$$\mathbf{D} = (0, 0, 0, \vec{\nabla}(\mathbf{K}h\vec{\nabla}\phi))^{\mathrm{T}} \tag{3}$$

$$\mathbf{R} = (0, -ghS_{fx}, -ghS_{fy}, 0)^{\mathrm{T}}$$

where the bed slopes are functions of the bottom level z,

$$S_{ox} = -\frac{\partial z}{\partial x}, \qquad S_{oy} = -\frac{\partial z}{\partial y} \tag{4}$$

and the friction losses are described in terms of the Manning's roughness coefficient n [18]:

$$S_{fx} = \frac{n^2 u\sqrt{u^2 + v^2}}{h^{4/3}}, \qquad S_{fy} = \frac{n^2 v\sqrt{u^2 + v^2}}{h^{4/3}} \tag{5}$$

$\mathbf{K}$ is an empirical matrix that should not be confused with the turbulent diffusivity. In general, $\mathbf{K}$ incorporates dispersion due to differential advection as well as turbulent diffusion [1]. All the examples considered in this work are purely advective, that is, use $\mathbf{K} = 0$.

It is useful to rewrite (1) as

$$\frac{\partial \mathbf{U}}{\partial t} + \frac{\partial \mathbf{F}}{\partial x} + \frac{\partial \mathbf{G}}{\partial y} = \mathbf{S}(x, y, \mathbf{U}) \tag{6}$$

The integral form of the equations over a fixed volume Ω,

$$\frac{\partial}{\partial t}\int_\Omega \mathbf{U}\,\mathrm{d}\Omega + \int_\Omega \left(\frac{\partial \mathbf{F}}{\partial x} + \frac{\partial \mathbf{G}}{\partial y}\right)\mathrm{d}\Omega = \int_\Omega \mathbf{S}\,\mathrm{d}\Omega \tag{7}$$

that, after application of Gauss's theorem to the second integral leads to

$$\frac{\partial}{\partial t}\int_\Omega \mathbf{U}\,\mathrm{d}\Omega + \oint_{\partial\Omega} (\mathbf{En})\,\mathrm{d}l = \int_\Omega \mathbf{S}\,\mathrm{d}\Omega \tag{8}$$

in which $\mathbf{E}$ is the 4×2 flux tensor $\mathbf{E} = (\mathbf{F}, \mathbf{G})$, $\mathbf{n}$ is the unit outward normal vector to the cell so that $\mathbf{En} = \mathbf{F}n_x + \mathbf{G}n_y$. $\partial\Omega$ denotes the surface surrounding the volume Ω.

NUMERICAL METHOD

In the two-dimensional approach presented in this work, the spatial domain of integration is covered by a set of unstructured triangular cells, and a cell-centred finite volume method is formulated where all the dependent variables of the system are represented as piecewise constant per cell. A discrete approximation of (8) is applied in every cell Ω_i at a given time so that the volume integrals represent integrals over the area of the cell and the surface integrals represent the normal flux through the cell boundaries. Denoting by $\mathbf{U}_i$ the cell-average value of the conservative variables in cell Ω_i at a given time, from (8) the following conservation equation can be written for every cell:

$$\frac{\partial \mathbf{U}_i}{\partial t} A_i + \oint_{\partial\Omega} (\mathbf{En})\, \mathrm{d}l = \int_{\Omega} \mathbf{S}\, \mathrm{d}\Omega \tag{9}$$

where A_i is the area of the cell Ω_i. The normal flux at the edge of the cells is approximated by

$$\oint_{\partial\Omega_i} (\mathbf{En})\, \mathrm{d}l \approx \sum_{k=1}^{\mathrm{NE}} (\delta \mathbf{En})_{i,k} l_k, \qquad (\delta \mathbf{En})_{i,k} = (\mathbf{E}_j - \mathbf{E}_i)\mathbf{n}_{i,k} \tag{10}$$

as a starting point for the derivation of the first-order flux difference splitting technique, where k represents the index of the edge shared between cells Ω_i and Ω_j, the vector $\mathbf{n}_{i,k}$ is the unit outward normal in cell Ω_i on edge k, l_k is the length of the edge k, (Figure 1), $(\delta \mathbf{En})_{i,k}$ is the numerical flux difference across the cell edge, $\mathbf{E}_j$ and $\mathbf{E}_i$ are evaluated at cells j and i, and NE is the number of edges that define the cell. The problem is then reduced to a one-dimensional Riemann problem projected in the direction $\mathbf{n}_{i,k}$ at each cell edge [24]. Roe [25] defined an approximated flux Jacobian, $\widetilde{\mathbf{J}}_{\mathbf{n}_{i,k}}$ for the Euler equations, and an approximate flux Jacobian

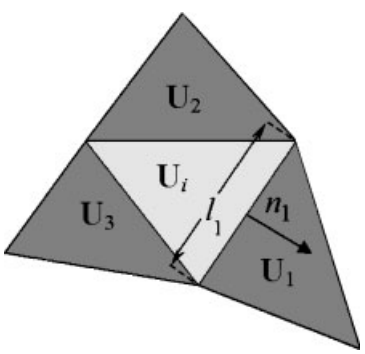

Figure 1.

for the coupled system shallow flow/solute transport can be defined [23],

$$\delta(\mathbf{En})_{i,k} = \widetilde{\mathbf{J}}_{\mathbf{n}_{i,k}} \delta \mathbf{U}_{i,k} \tag{11}$$

with the following eigenvalues:

$$\begin{aligned} \widetilde{\lambda}^1_{i,k} &= (\widetilde{\mathbf{u}} \cdot \mathbf{n} + \widetilde{c})_{i,k} \\ \widetilde{\lambda}^2_{i,k} &= (\widetilde{\mathbf{u}} \cdot \mathbf{n})_{i,k} \\ \widetilde{\lambda}^3_{i,k} &= (\widetilde{\mathbf{u}} \cdot \mathbf{n} - \widetilde{c})_{i,k} \\ \widetilde{\lambda}^4_{i,k} &= (\widetilde{\mathbf{u}} \cdot \mathbf{n})_{i,k} \end{aligned} \tag{12}$$

and the corresponding eigenvectors

$$\widetilde{\mathbf{e}}^1_{i,k} = \begin{pmatrix} 1 \\ \widetilde{u} + \widetilde{c} n_x \\ \widetilde{v} + \widetilde{c} n_y \\ \widetilde{\phi} \end{pmatrix}_{i,k}, \quad \widetilde{\mathbf{e}}^2_{i,k} = \begin{pmatrix} 0 \\ -\widetilde{c} n_y \\ \widetilde{c} n_x \\ 0 \end{pmatrix}_{i,k}, \quad \widetilde{\mathbf{e}}^3_{i,k} = \begin{pmatrix} 1 \\ \widetilde{u} - \widetilde{c} n_x \\ \widetilde{v} - \widetilde{c} n_y \\ \widetilde{\phi} \end{pmatrix}_{i,k}, \quad \widetilde{\mathbf{e}}^4_{i,k} = \begin{pmatrix} 0 \\ 0 \\ 0 \\ 1 \end{pmatrix}_{i,k} \tag{13}$$

where

$$\begin{aligned} \widetilde{u}_{i,k} &= \frac{u_i \sqrt{h_i} + u_j \sqrt{h_j}}{\sqrt{h_i} + \sqrt{h_j}}, \quad \widetilde{v}_{i,k} = \frac{v_i \sqrt{h_i} + v_j \sqrt{h_j}}{\sqrt{h_i} + \sqrt{h_j}} \\ \widetilde{c}_{i,k} &= \sqrt{g \frac{h_i + h_j}{2}}, \quad \widetilde{\phi}_{i,k} = \frac{\phi_i \sqrt{h_i} + \phi_j \sqrt{h_j}}{\sqrt{h_i} + \sqrt{h_j}} \end{aligned} \tag{14}$$

Following a flux difference procedure, the difference in vector $\mathbf{U}$ across the grid edge is projected onto the matrix eigenvectors basis as

$$\delta \mathbf{U}_{i,k} = \sum_{m=1}^{4} (\alpha \widetilde{\mathbf{e}})^m_{i,k} \tag{15}$$

where the expression of coefficients $\alpha^m_{i,k}$ are

$$\begin{aligned} \alpha^{1,3}_{i,k} &= \frac{\delta h_{i,k}}{2} \pm \frac{1}{2\widetilde{c}_{i,k}} (\delta \mathbf{q}_{i,k} - \widetilde{\mathbf{u}}_{i,k} \delta h_{i,k}) \mathbf{n}_{i,k}, \quad \alpha^2_{i,k} = \frac{1}{\widetilde{c}_{i,k}} (\delta \mathbf{q}_{i,k} - \widetilde{\mathbf{u}}_{i,k} \delta h_{i,k}) \mathbf{n}_{i,k_t} \\ \alpha^4_{i,k} &= \delta(h\phi)_{i,k} - \widetilde{\phi} (\delta h)_{i,k} \end{aligned} \tag{16}$$

where $\mathbf{q} = (q_x, q_y)$ and $\mathbf{n}_t = (-n_y, n_x)$ is the tangential vector to the edge.

The flux difference across each edge k is split into contributions going in and out of every cell

$$\delta(\mathbf{En})_{i,k} = \sum_{m=1}^{4} (\widetilde{\lambda} \alpha \widetilde{\mathbf{e}})^{-m}_{i,k} + \sum_{m=1}^{4} (\widetilde{\lambda} \alpha \widetilde{\mathbf{e}})^{+m}_{i,k} \tag{17}$$

according to the sign of the eigenvalues of the normal flux Jacobian, where $\widetilde{\lambda}^{\pm m} = \frac{1}{2}(\widetilde{\lambda}^m \pm |\widetilde{\lambda}^m|)$, and, for the updating of every cell, only the in-going contributions generated at the edges surrounding it are of interest.

The discretization of the bottom elevation source terms is successfully constructed when it ensures an exact balance between flux gradients and bed variations [26, 27]. It has been demonstrated that, in first-order finite volume schemes, if the upwind technique is applied to the flux and bottom terms, in the case of still water, equilibrium is maintained for the water level surface [18, 28]. The same technique extended to the coupled system of equations provides equilibrium for the solute concentration [23]. For that purpose, the bottom source term is first approximated projecting it onto the basis of eigenvectors:

$$\int_\Omega \mathbf{B}\,\mathrm{d}\Omega \cong \sum_{k=1}^{\mathrm{NE}} \mathbf{B}_{i,k} = \sum_{k=1}^{\mathrm{NE}} \sum_{m=1}^{4} (\beta\widetilde{\mathbf{e}})_{i,k}^m l_k \tag{18}$$

where

$$\beta_{i,k}^l = \tfrac{1}{2}\widetilde{c}_{i,k}(-\delta z_{i,k}), \quad \beta_{i,k}^2 = 0, \quad \beta_{i,k}^3 = -\beta_{i,k}^1, \quad \beta_{i,k}^4 = 0 \tag{19}$$

and next splitting it in in-going and out-going contributions as was done with the flux difference:

$$\sum_{m=1}^{4} (\beta\,\widetilde{\mathbf{e}})_{i,k} l_k = \sum_{m=1}^{4} (\beta^- \widetilde{\mathbf{e}})_{i,k}^m l_k + \sum_{m=1}^{4} (\beta^+ \widetilde{\mathbf{e}})_{i,k}^m l_k \tag{20}$$

with $\beta^{\pm m} = \frac{1}{2}\beta^m(1 \pm \mathrm{sgn}(\widetilde{\lambda}^m))$.

At this point, Equation (9) becomes

$$\frac{\Delta \mathbf{U}_i}{\Delta t} A_i + \sum_{k=1}^{\mathrm{NE}} \sum_{m=1}^{4} ((\widetilde{\lambda}\alpha - \beta)\,\widetilde{\mathbf{e}})_{i,k}^{-m} l_k = \int_\Omega (\mathbf{R} + \mathbf{D})\,\mathrm{d}\Omega \tag{21}$$

that can be rewritten in a more compact form:

$$\frac{\Delta \mathbf{U}_i}{\Delta t} A_i + \sum_{k=1}^{\mathrm{NE}} \sum_{m=1}^{4} (\lambda^*\,\delta\mathbf{U})_{i,k}^m l_k = \int_\Omega (\mathbf{R} + \mathbf{D})\,\mathrm{d}\Omega \tag{22}$$

where $\lambda_{i,k}^{*m} = (\widetilde{\lambda} - \beta/\alpha)_{i,k}^{-m}$ and $\delta\mathbf{U}_{i,k}^m = (\alpha\widetilde{\mathbf{e}})_{i,k}^m$. When $\alpha_{i,k}^m$ is nil, $\lambda_{i,k}^{*m}\delta(\mathbf{U}) = -(\beta\mathbf{e})_{i,k}^m$.

The friction term $\mathbf{R}$ is discretized in a semi-implicit pointwise manner to avoid numerical oscillations [19], $\mathbf{R}_i = \mathbf{R}_i(\theta)$ (explicit with $\theta = 1$, and implicit with $\theta = 0$). The diffusion term is discretized implicitly [23] so the final expression for the complete numerical scheme is

$$\mathbf{U}_i^{n+1} = \mathbf{U}_i^n - \sum_{k=1}^{\mathrm{NE}} \sum_{m=1}^{4} (\lambda^*\delta\mathbf{U})_{i,k}^m \frac{l_k}{A_i}\Delta t + (\mathbf{R}_i(\theta) + \mathbf{D}_i^{n+1})\Delta t \tag{23}$$

We shall concentrate on the bed slope source terms letting aside the considerations concerning the friction and diffusion terms. In absence of friction and solute diffusion, the scheme

can be expressed as

$$
\begin{aligned}
h_i^{n+1} &= h_i^n + \Delta t \sum_{k=1}^{\mathrm{NE}} \Psi_{i,k}^h, \quad \Psi_{i,k}^h = \sum_{m=1}^{4} \psi_{i,k}^{m,h}, \quad \psi_{i,k}^{m,h} = -(\lambda^* \delta \mathrm{U}_1)_{i,k}^{-m} \frac{l_k}{A_i} \\
(hu)_i^{n+1} &= (hu)_i^n + \Delta t \sum_{k=1}^{\mathrm{NE}} \Psi_{i,k}^{hu}, \quad \Psi_{k,i}^{hu} = \sum_{m=1}^{4} \psi_{i,k}^{m,hu}, \quad \psi_{i,k}^{m,hu} = -(\lambda^* \delta \mathrm{U}_2)_{i,k}^{-m} \frac{l_k}{A_i} \\
(hv)_i^{n+1} &= (hv)_i^n + \Delta t \sum_{k=1}^{\mathrm{NE}} \Psi_{i,k}^{hv}, \quad \Psi_{i,k}^{hv} = \sum_{m=1}^{4} \psi_{i,k}^{m,hv}, \quad \psi_{i,k}^{m,hv} = -(\lambda^* \delta \mathrm{U}_3)_{i,k}^{-m} \frac{l_k}{A_i} \\
(h\phi)_i^{n+1} &= (h\phi)_i^n + \Delta t \sum_{k=1}^{\mathrm{NE}} \Psi_{i,k}^{h\phi}, \quad \Psi_{i,k}^{h\phi} = \sum_{m=1}^{4} \psi_{i,k}^{m,h\phi}, \quad \psi_{i,k}^{m,h\phi} = -(\lambda^* \delta \mathrm{U}_4)_{i,k}^{-m} \frac{l_k}{A_i}
\end{aligned}
\tag{24}
$$

It must be signalled that (24) is formally different to the usual finite volume formulation in which numerical fluxes are defined at the edges. In (24), fluxes and slope source terms participate in a unified form that is controlled by the redefined eigenvalues $\lambda_{i,k}^{*m}$.

It is well known that, when using Roe's linearization, the approximate eigenvalues must be modified in the case of sonic rarefactions in order to avoid nonphysical solutions. According to the ideas proposed by Harten and Hyman [29]:

$$
\begin{aligned}
\sigma &= \frac{\lambda_j^m(\mathbf{n}_{i,k}) - \widetilde{\lambda}_{i,k}^m}{\lambda_j^m(\mathbf{n}_{i,k}) - \lambda_i^m(\mathbf{n}_{i,k})} \\
\widetilde{\lambda}_{i,k}^m &= \begin{cases} \lambda_i^m(\mathbf{n}_{i,k})\sigma & \text{if } \lambda_i^m(\mathbf{n}_{i,k}) < 0 < \lambda_j^m(\mathbf{n}_{i,k}) \text{ for } m = 1 \text{ or } 3 \\ \widetilde{\lambda}_{i,k}^m & \text{otherwise} \end{cases}
\end{aligned}
\tag{25}
$$

where $\lambda_i^m = \lambda_i^m(\mathbf{U}_i)$ and $\lambda_j^m = \lambda_j^m(\mathbf{U}_j)$.

This correction modifies the waves at the cell edges and, therefore, a corresponding modification of the redefined eigenvalues becomes necessary

$$
\lambda_{i,k}^{*m} = \begin{cases} \left(\lambda_i^m - \dfrac{\beta_{i,k}^m}{\alpha_{i,k}^m}\right)\sigma & \text{if } \lambda_i^m(\mathbf{n}_{i,k}) < 0 < \lambda_j^m(\mathbf{n}_{i,k}) \text{ for } m = 1 \text{ or } 3 \\ \lambda_{i,k}^{*m} & \text{otherwise} \end{cases}
\tag{26}
$$

where σ is computed as in (25). This is the only way to ensure a conservative entropy satisfaction when sonic rarefactions occur. An example of the necessity of applying this correction will be shown in the 'numerical results' Section.

SOLUTE CONCENTRATION CONSTRAINTS

In the coupled system of equations (2), the conserved variable is $h\phi$ so that the value of solute concentration ϕ is computed as a ratio between the conserved solute mass and the water depth. This can lead to unbounded and unrealistic values in the final solute concentration when the

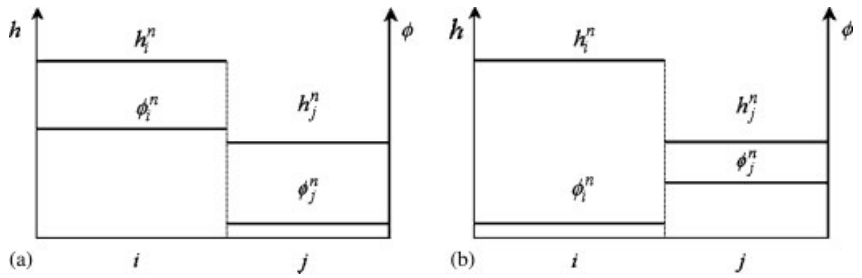

Figure 2. Sketch of two possible situations that may lead to oscillations in the solute concentration solution.

eigenvalues associated to the normal velocity do not update the solution in the future time:

$$\widetilde{\lambda}_{i,k}^{-2} = \widetilde{\lambda}_{i,k}^{-4} = (\widetilde{\mathbf{un}})_{i,k}^{-} = 0 \tag{27}$$

as solute transport is exclusively produced by the water mass movement. Two cases which produce oscillations in the solute concentration have been identified.

Figure 2(a) describes one case: the water depth h and solute concentration ϕ at cell i is bigger than the solute concentration value at cell j and the incoming normal Roe's averaged velocity to cell i is nil, $(\widetilde{\mathbf{un}})_{i,k}^{-} = 0$, which implies $\Psi_{i,k}^{h\phi} = \widetilde{\phi}_{i,k}\Psi_{i,k}^{h}$. Furthermore, the updating water mass flux to cell i is negative, $\Psi_{i,k}^{h} < 0$, so that $h_i^n > h_i^{n+1}$, as in this case only the interaction between cells i and j is allowed. The updated value of solute concentration at cell i must be bounded by:

$$\phi_i^{n+1} = \frac{(h\phi)_i^n + \Psi_{i,k}^{h\phi}\,\Delta t}{h_i^{n+1}} = \frac{(h\phi)_i^n + \widetilde{\phi}_{i,k}\Psi_{i,k}^{h}\,\Delta t}{h_i^{n+1}} = r\phi_i^n + (1-r)\,\widetilde{\phi}_{i,k} < \phi_i^n, \quad r = \frac{h_i^n}{h_i^{n+1}} > 1 \tag{28}$$

which is equivalent to

$$(1-r)\,\widetilde{\phi}_{i,k} < (1-r)\phi_i^n \tag{29}$$

and considering that $(1-r) \leqslant 0$

$$\widetilde{\phi}_{i,k} > \phi_i^n \tag{30}$$

condition that can never be met as

$$\widetilde{\phi}_{i,k} < \phi_{\max} = \phi_i^n \tag{31}$$

Figure 2(b) describes the other case: the solute concentration ϕ at cell i is smaller than the solute concentration ϕ at cell j. Also $(\widetilde{\mathbf{un}})_{i,k}^{-} = 0$ and $\Psi_{i,k}^{h} < 0$. The value of updated solute concentration at cell i must be bounded by the minimum concentration ϕ_i^n, and according to the definitions in (28):

$$\phi_i^{n+1} = r\phi_i^n + (1-r)\widetilde{\phi}_{i,k} > \phi_i^n \tag{32}$$

This result can be rewritten as

$$(1-r)\,\widetilde{\phi}_{i,k} > (1-r)\phi_i^n \tag{33}$$

or considering that $(1-r) \leqslant 0$

$$\widetilde{\phi}_{i,k} < \phi_i^n \tag{34}$$

condition that can never be met as

$$\widetilde{\phi}_{i,k} > \phi_{\min} = \phi_i^n \tag{35}$$

In this work, a strategy that avoids these situations by enforcing a conservative redistribution of the solute mass fluxes is presented. A virtual solute concentration ϕ_V is defined for that purpose at each cell edge between cells i and j

$$\phi_V = \begin{cases} \max\{\phi_i, \phi_j\} & \text{if } \delta\phi_{i,k}^n < 0 \\ \min\{\phi_i, \phi_j\} & \text{if } \delta\phi_{i,k}^n > 0 \end{cases} \tag{36}$$

with $\delta\phi_{i,k}^n = \phi_j^n - \phi_i^n$, so that, in general, in those cases where $\Psi_{i,k}^h < 0$ and $\widetilde{\lambda}_{i,k}^{-4} = 0$ the solute mass flux updating cell i coming from edge k, $\Psi_{i,k}^{h\phi}$, and that updating cell j coming from the same edge interface, $\Psi_{i,k}^{h\phi}$, are redefined as

$$\begin{aligned} &\Psi_{i,k}^{h\phi} = \phi_V \Psi_{i,k}^h \\ &\Psi_{j,k}^{h\phi} = \Psi_{j,k}^{h\phi} + (\widetilde{\phi}_k - \phi_V)\Psi_{i,k}^h r_A, \quad \Psi_{i,k}^h < 0, \quad \lambda_{i,k}^{-4} = 0 \end{aligned} \tag{37}$$

with $r_A = A_i/A_j$, to preserve conservation.

NUMERICAL STABILITY

The basic method used to determine the maximum time step size compatible with numerical stability in hyperbolic problems only addresses the linear homogeneous case and takes into account the influence of the eigenvalues of the Jacobian matrix and the mesh geometry [30]. The influence of the source terms is not traditionally considered when the time step is chosen. In this paper, the influence of those terms within the coupled system will be studied. In general, to generate the criterion for calculating the maximum time step size compatible with numerical stability in a hyperbolic problem, a homogeneous linear scalar equation is used:

$$\frac{\partial u}{\partial t} + \boldsymbol{\lambda}\vec{\nabla}u = 0 \tag{38}$$

with $\boldsymbol{\lambda} = (\lambda_x, \lambda_y)$. The updating formula for each cell i using the first-order upwind finite volume method is

$$u_i^{n+1} = u_i^n - \sum_{k=1}^{\mathrm{NE}} (\boldsymbol{\lambda}\mathbf{n})_{i,k}^- \delta u_{i,k} \Delta t \frac{l_k}{A_i} \tag{39}$$

To ensure conservation, it is necessary that the cells in the domain are such that the following condition holds [24]:

$$\sum_{k=1}^{\mathrm{NE}} \mathbf{n}_{i,k} l_k = 0 \tag{40}$$

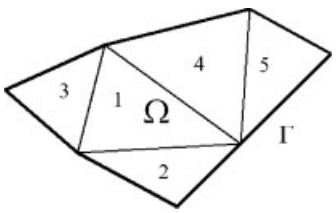

Figure 3. Mesh discretization.

This can be illustrated using the upwind finite volume scheme. The scheme is conservative if the sum of the total computed waves at the internal cell interfaces is equal to the balance of fluxes that cross the boundary of the domain, that is to say

$$\underbrace{\sum_{i=1}^{\text{Ncell}} \sum_{k\in k_\Omega} ((\boldsymbol{\lambda}\mathbf{n})^- \delta u\, l)_{i,k}}_{C\Omega} = \underbrace{\int_\Gamma (\boldsymbol{\lambda}\mathbf{n}) u \,\mathrm{d}l}_{C\Gamma} = \sum_{i=1}^{\text{Ncell}} \sum_{k\in k_\Gamma} (\underbrace{(\boldsymbol{\lambda}\mathbf{n})^- u\, l)_{i,k}}_{\text{ingoing flow}} + \underbrace{((\boldsymbol{\lambda}\mathbf{n})^+ u\, l)_{i,k}}_{\text{outgoing flow}} \tag{41}$$

where k_Ω are the edges inside the domain, and k_Γ are the edges that shape the contour boundary. For the sake of clarity, (41) will be proved in the domain represented by Figure 3.

To illustrate this example, the notation used for the updating waves at the edges, i,k, will be changed by i, j, where j is the cell that shares the interface edge k. The total wave contributions at the inner cell edges is equal to

$$\begin{aligned} C\Omega = {} & ((\boldsymbol{\lambda}\mathbf{n})^- \delta u\, l)_{1,2} + ((\boldsymbol{\lambda}\mathbf{n})^- \delta u\, l)_{1,3} + ((\boldsymbol{\lambda}\mathbf{n})^- \delta u\, l)_{1,4} \\ & + ((\boldsymbol{\lambda}\mathbf{n})^- \delta u\, l)_{2,1} + ((\boldsymbol{\lambda}\mathbf{n})^- \delta u\, l)_{3,1} + ((\boldsymbol{\lambda}\mathbf{n})^- \delta u\, l)_{4,1} \\ & + ((\boldsymbol{\lambda}\mathbf{n})^- \delta u\, l)_{4,5} + ((\boldsymbol{\lambda}\mathbf{n})^- \delta u\, l)_{5,4} \end{aligned} \tag{42}$$

where $\delta u_{i,j} = u_j - u_i$, $\mathbf{n}_{i,j}$ is the normal vector to the edge k directed from i to j, and $l_{i,j}$ is the length of the edge. Taking into account that $(\boldsymbol{\lambda}\mathbf{n})^-_{i,j} - (\boldsymbol{\lambda}\mathbf{n})^-_{j,i} = (\boldsymbol{\lambda}\mathbf{n})_{i,j}$, $(\boldsymbol{\lambda}\mathbf{n})^-_{i,j} + (\boldsymbol{\lambda}\mathbf{n})^+_{i,j} = (\boldsymbol{\lambda}\mathbf{n})_{i,j}$ and $\delta u_{i,j} = -\delta u_{j,i}$, (42) becomes

$$C\Omega = ((\boldsymbol{\lambda}\mathbf{n})\, \delta u\, l)_{1,2} + ((\boldsymbol{\lambda}\mathbf{n})\, \delta u\, l)_{1,3} + ((\boldsymbol{\lambda}\mathbf{n})\, \delta u\, l)_{1,4} + (\boldsymbol{\lambda}\mathbf{n})\, \delta u\, l)_{4,5} \tag{43}$$

which can be rewritten as

$$C\Omega = -(\boldsymbol{\lambda} u_1) \sum_{k=2}^{4} (\mathbf{n} l)_{1,k} + ((\boldsymbol{\lambda}\mathbf{n}) l)_{1,2} u_2 + ((\boldsymbol{\lambda}\mathbf{n}) l)_{1,3} u_3 + ((\boldsymbol{\lambda}\mathbf{n}) l)_{1,4} u_4 + ((\boldsymbol{\lambda}\mathbf{n})\, \delta u\, l)_{4,5} \tag{44}$$

Applying (40), the first term in (44) disappears, and

$$C\Omega = ((\boldsymbol{\lambda}\mathbf{n}) l)_{1,2} u_2 + ((\boldsymbol{\lambda}\mathbf{n}) l)_{1,3} u_3 + ((\boldsymbol{\lambda}\mathbf{n}) l)_{1,4} u_4 + ((\boldsymbol{\lambda}\mathbf{n})\, l)_{4,5} \delta u_{4,5} \tag{45}$$

On the other hand, the flow that crosses the contour can be computed as

$$C\Gamma = \sum_{k_\Gamma} ((\boldsymbol{\lambda}\mathbf{n}) l)_{2,k} u_2 + \sum_{k_\Gamma} ((\boldsymbol{\lambda}\mathbf{n}) l)_{3,k} u_3 + \sum_{k_\Gamma} ((\boldsymbol{\lambda}\mathbf{n}) l)_{4,k} u_4 + \sum_{k_\Gamma} ((\boldsymbol{\lambda}\mathbf{n}) l)_{5,k} u_5 \tag{46}$$

and, using (40):

$$\sum_{k_1} (\mathbf{n}l)_{i,k} + \sum_{k_\Omega} (\mathbf{n}l)_{i,k} = 0 \tag{47}$$

then, (46) can be rewritten

$$C\Gamma = -((\boldsymbol{\lambda}\mathbf{n})l)_{2,1}u_2 - ((\boldsymbol{\lambda}\mathbf{n})l)_{3,1}u_3 - ((\boldsymbol{\lambda}\mathbf{n})l)_{4,1}u_4 - ((\boldsymbol{\lambda}\mathbf{n})l)_{4,5}u_4 - ((\boldsymbol{\lambda}\mathbf{n})l)_{5,4}u_5 \tag{48}$$

or

$$C\Gamma = ((\boldsymbol{\lambda}\mathbf{n})l)_{1,2}u_2 + ((\boldsymbol{\lambda}\mathbf{n})l)_{1,3}u_3 + ((\boldsymbol{\lambda}\mathbf{n})l)_{1,4}u_4 + ((\boldsymbol{\lambda}\mathbf{n})l)_{4,5}\delta u_{4,5} \tag{49}$$

which is equal to (45), showing that condition (40) is essential to ensure conservation.

The updating formula in (39) can also be expressed in a compact form as

$$u_i^{n+1} = u_i^n - \sum_{k=1}^{\mathrm{NE}} v_{i,k}\delta u_{i,k} \tag{50}$$

where $v_{i,k} = \Delta t(\widetilde{\boldsymbol{\lambda}}\mathbf{n})_{i,k}^{-}(l_k/A_i)$ is a dimensionless quantity. To ensure numerical stability, $v_{i,k}$ must be limited [31] by

$$-1 \leqslant v_{i,k} \leqslant 0 \tag{51}$$

Given a grid mesh and flow conditions, (51) requires reducing the value of the time step to meet the stability criterion. As an example, let us assume that the u_j values are equal at all the surrounding cells to cell i, but different to u_i, with $u_i > u_j$ and $u_j > 0$. Using (40) in the case of a triangular cell, the incoming contributions to cell i described in (39) can be bounded:

$$\left|\sum_k (\boldsymbol{\lambda}\mathbf{n})_{i,k}^{-} l_k \delta u_{i,k}\Delta t\right| = \left|\sum_k ((\boldsymbol{\lambda}\mathbf{n})^{-}l)_{i,k}\right| \delta u_o \Delta t \leqslant \max_k (|\boldsymbol{\lambda}\mathbf{n}|l)\, \delta u_o \Delta t = (|\boldsymbol{\lambda}\mathbf{n}|l)_{k_{\max}} \delta u_o \Delta t \tag{52}$$

where $\delta u_o = \delta u_k$. And similarly in the case of a rectangular cell

$$\left|\sum_k ((\boldsymbol{\lambda}\mathbf{n})^{-}l)_{i,k}\right| \delta u_o \Delta t \leqslant 2 \max_k (|\lambda\mathbf{n}|l)\delta u_o \Delta t \tag{53}$$

since the updating contributions to a cell can at most enter through two edges.

Furthermore, the updating flux crossing edge k between cells i, j must be limited by the quantity that ensures that the final state at both cells is included between the initial values. This quantity can be computed as $\delta u_o \cdot \min\{A_i, A_j\}$, where A_i and A_j are the areas of cells i and j, respectively. Since all the incoming fluxes to cell i can be bounded according to (52), the following condition is stated:

$$\max_k (|\boldsymbol{\lambda}\mathbf{n}|l)\delta u_o\, \Delta t \leqslant \delta u_o \cdot \min\{A_i, A_j\}_{k_{\max}} \tag{54}$$

This leads to a stability constraint defined by cells. It is more feasible to define at each edge the quantity [31]

$$\Delta t_k = \frac{\min\{A_i, A_j\}}{(|\boldsymbol{\lambda}\mathbf{n}|l)_k} \tag{55}$$

for a triangular cell, or in the case of rectangular mesh

$$\Delta t_k = \frac{\min\{A_i, A_j\}}{2(|\boldsymbol{\lambda}\mathbf{n}|l)_k} \tag{56}$$

and to search the minimum among all of them, as a global limit for the time step in the mesh. This can be seen as the 2D extension of the classical Courant–Friedrichs–Lewy (CFL) condition for numerical stability of an explicit scheme [32].

Condition (56) can be generalized to a system of equations by extending the search over all the eigenvalues of the Jacobian as they play the role of advection velocities. In that case:

$$\Delta t_{\max,k} = \min\left\{\frac{\min\{A_i, A_j\}}{(|\widetilde{\lambda}^m(\mathbf{n})|l)_{i,j}}\right\}_{m=1,\ldots,N_\lambda}$$

$$\Delta t_{\max} = \min\{\Delta t_{\max,k}\}_{k=1,\,\mathrm{NEDGE}} \tag{57}$$

where the N_λ is the number of eigenvalues of the Jacobian matrix and NEDGE is the number of interior edges in the mesh. Also, a reduction factor of 2 must be applied if rectangular cells are used. Using (57), the following condition is ensured:

$$-1 \leqslant v_k^m \leqslant 0, \quad m = 1, \ldots, N_\lambda \tag{58}$$

where $v_k = \Delta t(\boldsymbol{\lambda}^m(\mathbf{n}))_k^-(l_k/A_i)$, keeping the numerical scheme stable [31].

The limits given by (55) or (57) over the time step can control properly the numerical stability when dealing with gradually varied functions in which $\delta u < u_i, u_j$. In general cases in which either the jump in the variable is finite or one of the values u_i, u_j may be zero at some cells, the restriction may not be sufficient and (54) must be redefined as follows:

$$(|\boldsymbol{\lambda}\mathbf{n}|l)\delta u_o \Delta t \leqslant \min\{\delta u_o, u_i, u_j\} \cdot \min\{A_i, A_j\} \tag{59}$$

or

$$(|\boldsymbol{\lambda}\mathbf{n}|l)\,\delta u_o \Delta t \leqslant \gamma \delta u_o \min\{A_i, A_j\} \tag{60}$$

with:

$$\gamma = \frac{\min\{u_i, u_j, \delta u_o\}}{\delta u_o}, \quad 0 \leqslant \gamma \leqslant 1 \tag{61}$$

This leads to a stronger stability constraint defined by cells for those cases where $\gamma \neq 0$

$$\Delta t_k = \gamma\,\frac{\min\{A_i, A_j\}}{(|\boldsymbol{\lambda}\mathbf{n}|l)_k} \tag{62}$$

with a reduction factor equal to 2 in the case of rectangular cells. From (60), in the case of $\gamma = 0$, the following well-known upwind condition over the updating fluxes derives:

$$(\boldsymbol{\lambda}\mathbf{n})_k^- \leqslant 0 \tag{63}$$

that is independent of the time step and correctly discriminates the cell edges allowed to transfer updating information into the cell. This can also be demonstrated considering the

updating fluxes in the following case: assume the value of u at cell i is positive, $u_i > 0$ and at the other side of edge k, the value of u is $u_j = 0$. The updating flux should lead to a decrease in the magnitude of u_i, from (50)

$$-v_{i,k}\delta u_{i,k} \leqslant 0 \tag{64}$$

and the final value at cell j would be $u_j \geqslant 0$, from (50)

$$-v_{j,k}\delta u_{j,k} \geqslant 0 \tag{65}$$

As $\delta u_{i,k} < 0$ and $\delta u_{j,k} > 0$, (64) can be rewritten as

$$v_{i,k} = (\lambda \mathbf{n})^{-}_{i,k} \frac{l_k}{A_i} \Delta t \leqslant 0 \tag{66}$$

and (65):

$$v_{j,k} = (\lambda \mathbf{n})^{-}_{j,k} \frac{l_k}{A_j} \Delta t \leqslant 0 \tag{67}$$

both of them equivalent to (63).

The generalization to a system of equations provides a new condition:

$$\begin{gathered} \Delta t_{\max,k} = \min \left\{ \gamma \frac{\min\{A_i, A_j\}}{(|\widetilde{\lambda}^m(\mathbf{n})|l)_k} \right\}_{m=1,\ldots,N_\lambda} \\ \gamma = \min_n \left\{ \frac{\min_{i,j}\{U_{n,i}, U_{n,j}, |\delta U_n|\}}{|\delta U_n|} \right\} \leqslant 1, \qquad \mathbf{U} = (U_1, \ldots, U_n, \ldots, U_{nc})^{\mathrm{T}} \\ \Delta t_{\max} = \min\{\Delta t_{\max,k}\}_{k=1,\mathrm{NEDGE}} \end{gathered} \tag{68}$$

This condition can lead to overly restrictive time step sizes as γ tends to zero. Our goal is to be able to rely on condition (57) for numerical stability even in presence of wetting/drying processes such as those making γ go to zero. These situations, based on (63), can be identified by

$$\widetilde{\lambda}_k^{-m}(\mathbf{n}) \leqslant 0, \quad m = 1, \ldots, N_\lambda \tag{69}$$

Equation (63) in the scalar case, or (69) in the case of systems will be used to design an algorithm able to ensure stability using condition (57) for the time step. This will be detailed in next section in the context of the coupled shallow-water transport system with source terms.

STABILITY CRITERION: APPLICATION TO THE COUPLED SHALLOW-WATER EQUATION IN REAL SCENARIOS

The stability region defined according to (57) and using the λ^m eigenvalues of the approximate Jacobian, (12) is appropriate to accurately define the time step in flow problems where bed slope source terms are not dominant and where there is a fixed flow domain. But this stability

region fails in the case of wetting/drying fronts, as reported [18] and (68) becomes necessary to redefine the stability region. This can be re-expressed with the help of the redefined λ_k^{*m} eigenvalues, leading to

$$\Delta t_{\max,k} = \min\left\{ \gamma \frac{\min\{A_i, A_j\}}{(|\lambda^{*m}|l)_{i,k}} \right\}_{m=1,\ldots,4}$$
$$\Delta t_{\max} = \min\{\Delta t_{\max,k}\}_{k=1,\mathrm{NEDGE}} \tag{70}$$

It must be signalled that in the set of conserved variables only water depth and solute mass are relevant to compute the value of γ, as their positivity property must be guaranteed in all cases:

$$\gamma = \min\left\{ \frac{\min\{h_i, h_j, |\delta h|\}}{|\delta h|}, \frac{\min\{(h\phi)_i, (h\phi)_j, |\delta(h\phi)|\}}{|\delta(h\phi)|} \right\} \tag{71}$$

also, in wetting front advance, in which $\gamma = 0$, and condition (69) must be applied as

$$\lambda_k^{*m} \leqslant 0, \quad m = 1, \ldots, 4 \tag{72}$$

condition independent of the time step that plays the role of identifying the cell edges and wave components allowed to enter updating information into the cell in case of a system with source terms. This result includes the conditions defined to maintain equilibrium when wetting/drying interfaces appear in cases of still water [18] and flooding advance [19] where a redefinition of the bottom slopes was proposed to balance correctly the source terms. The clean/mixed water fronts can be also included in the definition of (72), but in these cases, where the water depth is positive in both sides of the edge k, it is sufficient to introduce the corrections defined in (37).

The generation of new dry areas from initially wet zones leads to almost nil values of water depth and solute mass during drying processes, generating values of $\gamma \ll 1$. The stability criterion defined in (70), although sufficient to control numerical stability, leads to strong restrictions in the magnitude of the time step and unacceptable computational costs in these cases, requiring an alternative strategy to overcome this situation. The strategy presented in this work is based on the redefinition of the bottom slopes, which is equivalent to redistribute the updating fluxes, by means of the dimensionless variable r_t, which involves two local time steps, $\Delta t_{h,i}$ and $\Delta t_{h\phi,i}$ and the global time step. The local time step $\Delta t_{h,i}$ is defined to force nonnegative values of water depth at a new time level, h_i^{n+1} at every cell i: $\Delta t_{h,i}$ is computed involving the contributions from neighbour cells that extract mass, that is, that decrease the water depth in the wet cell i. With reference to (24) $\Delta t_{h,i}$ is computed as

$$\Delta t_{h,i} = -\frac{h_i^n}{\sum_{k=1}^{\mathrm{NE}} \Psi_{i,k}^h}, \quad \Psi_{i,k}^h \leqslant 0 \tag{73}$$

The local time step $\Delta t_{h\phi,i}$ is generated to avoid negatives values of solute mass, and is computed as:

$$\Delta t_{h\phi,i} = -\frac{(h\phi)_i^n}{\sum_{k=1}^{\mathrm{NE}} \Psi_{i,k}^{h\phi}}, \quad \Psi_{i,k}^{h\phi} \leqslant 0 \tag{74}$$

It is worth noting that the quantities defined in (73) and (74) are always positive due to the condition on the contributions in the denominator. Finally, the redistribution factor is computed as

$$r_{t,i} = \frac{\Delta t_v}{\Delta t_{\max}} \leqslant 1, \quad \Delta t_v = \min\{\Delta t_{\max}, \Delta t_{h,i}, \Delta t_{h\phi,i}\} \tag{75}$$

where $\Delta t_{\max}$ as in (57). When in the cell i the ratio $r_{t,i} < 1$, we propose to redefine the updating fluxes to cells i and j at those k edges where $\Psi^h_{i,k} \leqslant 0$ according to:

$$\begin{aligned} &\Psi^h_{i,k} = \omega_{h1}, \quad \Psi^{h\phi}_{i,k} = \omega_{\phi 1} \\ &\Psi^h_{j,k} = \Psi^h_{j,k} + \omega_{h2}, \quad \Psi^{h\phi}_{j,k} = \Psi^{h\phi}_{j,k} + \omega_{\phi 2} \\ &\Psi^{hu}_{i,k} = \Psi^{hv}_{i,k} = 0 \end{aligned} \tag{76}$$

where, to preserve conservation, the quantities ω_{h1}, ω_{h2}, $\omega_{\phi 1}$, $\omega_{\phi 2}$ are

$$\begin{aligned} &\omega_{h1} = \Psi^h_{i,k} r_{t,i}, \quad \omega_{h2} = \Psi^h_{i,k}(1 - r_{t,i}) r_A \\ &\omega_{\phi 1} = \Psi^{h\phi}_{i,k} r_{t,i}, \quad \omega_{\phi 2} = \Psi^{h\phi}_{i,k}(1 - r_{t,i}) r_A \end{aligned} \tag{77}$$

It is worth noting, for the sake of clarity, that the adjusted wave speeds λ^{*m}_k participate directly in the identification of the updating cell edges and wave components as well as in the computation of the updating quantities (24). However, it is important to stress that the goal of this method is to apply the largest possible time step compatible with stability, hence, condition (57) is established as the target value.

Also, it is important to remark, that the discrete source term coefficients β^1_k and β^3_k do not participate in the water and solute mass conservation equations when both associate eigenvalues $\widetilde{\lambda}^1_{i,k}$ and $\widetilde{\lambda}^3_{i,k}$ are negative. This situation can be defined when the local normal Froude number is

$$Fr_k = \left| \frac{\widetilde{\mathbf{u}}\mathbf{n}}{\widetilde{c}} \right|_k \geqslant 1 \tag{78}$$

COUPLED CONSERVATIVE SCHEME (CCS)

In order to handle transient inundation flows with solute transport properly, a modification of the numerical model defined by Equation (24), using the less restrictive time step limit (57), involving conditions required to stay conservative and stable have been presented. Finally, a complete summary of the steps conforming the CCS is presented including new conditions that will be explained below.

1. Compute the m λ^{*m}_k values and the respective $\psi^{m,h}_{i,k}$, $\psi^{m,hu}_{i,k}$, $\psi^{m,hv}_{i,k}$ $\psi^{m,h\phi}_{i,k}$ for each m wave at each edge cell k, as in (24), taking into account the entropy correction defined in (26).
2. If h^n_i or h^n_j are zero, $Fr_k < 1$ and $\lambda^{*m}_k > 0$, set

$$\psi^{m,h}_{i,k} = \psi^{m,hu}_{i,k} = \psi^{m,hv}_{i,k} = \psi^{m,h\phi}_{i,k} = 0 \quad \text{and impose } (\mathbf{u}_i \mathbf{n}_{i,k})^{n+1} = (\mathbf{u}_j \mathbf{n}_{i,k})^{n+1} = 0 \tag{79}$$

3. Update each $\Psi_{i,k}$ with its respective $\psi_{i,k}$'s.
4. If $h_i^n > 0$ and $h_j^n > 0$, $\Psi_{i,k}^h < 0$ and $\lambda_k^{-4} = 0$, redefine the respective $\Psi_{i,k}^{h\phi}$ and $\Psi_{j,k}^{h\phi}$ as indicated in (37).
5. Compute $\Delta t_{\max}$ as in (57).
6. For each cell i, define $r_{t,i}$ and, if $r_{t,i} < 1$, redefine the updating fluxes as in (76), setting, at those edges where $\Psi_{i,k}^h \leqslant 0$,

$$(\mathbf{u}_i \mathbf{n}_{i,k})^{n+1} = (\mathbf{u}_j \mathbf{n}_{i,k})^{n+1} = 0 \tag{80}$$

7. Update the conserved variables h_i^{n+1}, hu_i^{n+1}, hv_i^{n+1}, $h\phi_i^{n+1}$.
8. If $h_i^{n+1} < 0$ or $(h\phi)_i^{n+1} < 0$ set $\Delta t_{\max} = \frac{1}{2}\Delta t_{\max}$ and return to point 6.
9. At each edge: if $h_i = 0$ and $h_j > 0$, and $z_i > z_{j+} h_i = 0$ set:

$$\mathbf{u}_j \mathbf{n}_{j,k} = 0 \tag{81}$$

The reduction in the size of the time step in 8 is necessary in drying processes starting from almost null values of water depth, where the redefinition of the bottom slopes does not ensure positive values of water depth and solute mass. This reduction has an irrelevant computational cost, generating always a solution for the future time step. Also the imposition of zero normal velocities in 2, 6 and 9 is required to keep the numerical scheme conservative, as it avoids fluxes crossing those edges acting like solid boundaries.

NUMERICAL RESULTS

Circular dam break with nonuniform solute concentration

In order to analyse the quality of the numerical solution of the water flow and solute concentration variation in presence of strong gradients of water depth and solute mass, a circular dam break problem with nonuniform solute concentration is performed. A square frictionless and flat domain, $4000\,\mathrm{m} \times 4000\,\mathrm{m}$, is divided in triangular cells, created by dividing square elements along the top-left and top-right diagonal to the bottom, as Figure 4 shows, with $l = 25\,\mathrm{m}$. On a finer mesh the results are of better quality.

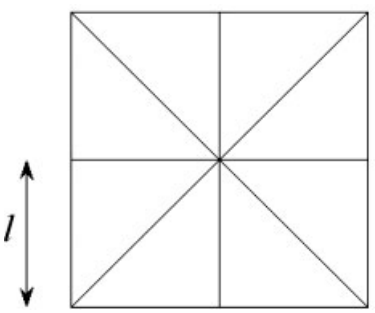

Figure 4. Cell triangulation.

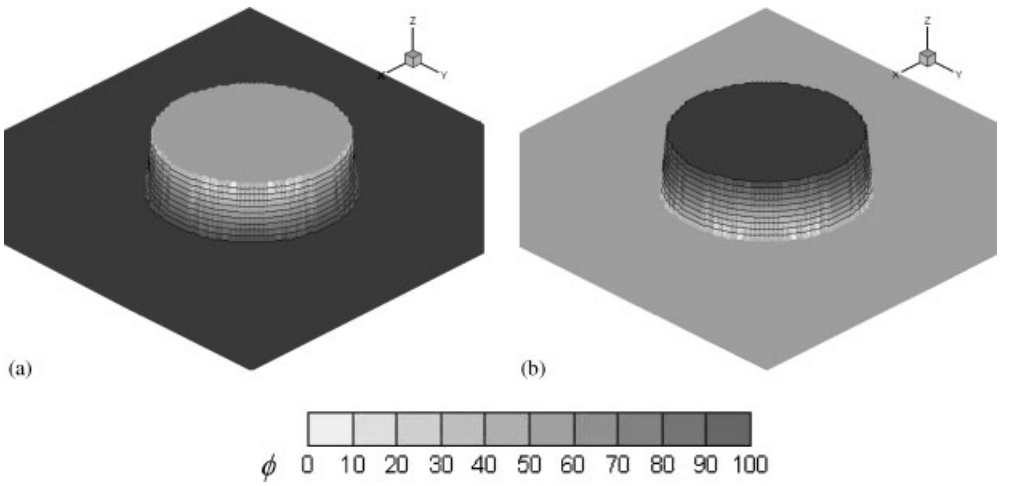

Figure 5. 3D view of the water level surface and a contour plot of the solute concentration: (a) for case (i); and (b) for case (ii).

The discontinuous initial water depth is defined by a radial function

$$h(r) = \begin{cases} 10, & r < 800 \\ 5, & r \geqslant 800 \end{cases} \tag{82}$$

where r is the distance from the centre of the domain. For that initial water-depth distribution two solute distributions are defined, the first test case (i) is

$$\phi(r) = \begin{cases} 0, & r < 800 \\ 100, & r \geqslant 800 \end{cases} \tag{83}$$

and the second test case (ii) is

$$\phi(r) = \begin{cases} 100, & r < 800 \\ 0, & r \geqslant 800 \end{cases} \tag{84}$$

Figure 5(a) displays a 3D view of the water level surface and a contour plot of the solute concentration for case (i) and Figure 5(b) displays the contour plot for case (ii).

These cases can be used to illustrate the overshoots and undershoots produced in the solute concentration when not applying (37) in presence of discontinuous water depth and solute concentration. Figure 6(a) displays the result for the maximum and minimum solute concentration when the dam break simulation is performed for case (i) in function of the simulated time. The maximum solute concentration is correctly bounded while the minimum solute concentration is smaller than the initial one. When the technique presented in (37) is applied, the minimum value remains bounded along the simulation, preserving conservation. On the other hand, Figure 6(b) shows the maximum and minimum solute concentration for case (ii) showing how the maximum allowable value in the solute concentration is overtopped. If the

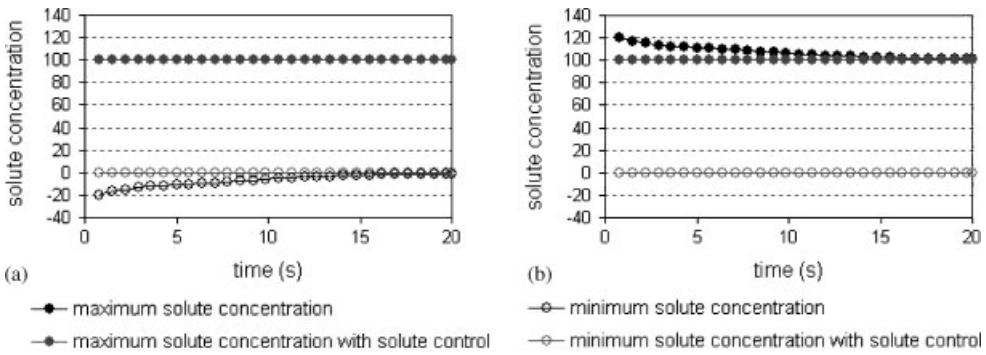

Figure 6. Maximum and minimum numerical solute concentration values in the dam break simulation using the basic scheme and controlling the solute concentration limits.

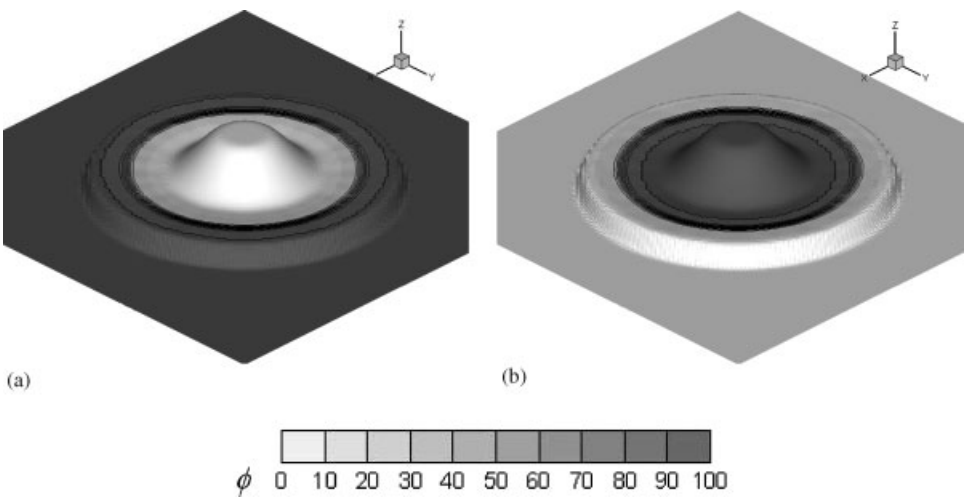

Figure 7. 3D view of the water level surface and a contour plot of the solute concentration: (a) for case (i); and (b) for case (ii) at $t = 50$ s.

technique presented in (37) is used, no overshoots in the solute concentration are observed along the simulation. Figure 7(a) and (b) display a 3D view of the dam break simulation at time $t = 50$ s and a contour plot of the solute concentration for case (i) and case (ii), respectively.

Static wet/dry boundary

In this numerical example, a simple case of still water over a variable bottom is analysed. Within the same closed-square basin of the previous test case, a square solid prism is placed surrounded by still water with concentration. The exact solution in this case is trivial and consists of unchanged initial conditions. The initial water surface level and the solute

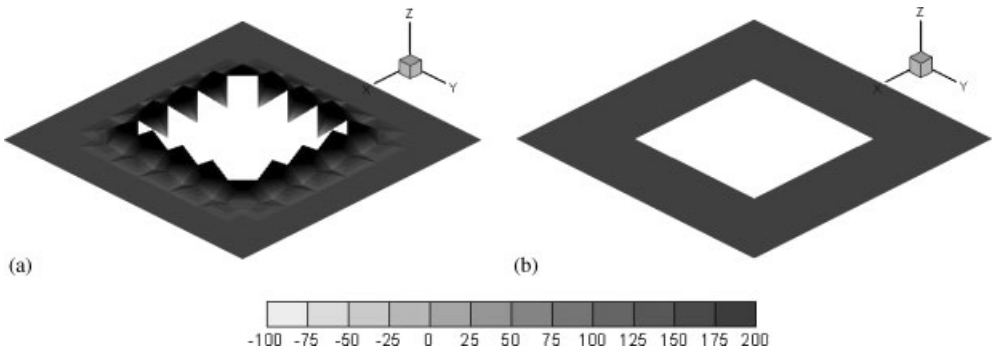

Figure 8. 3D view of the water depth and contour plot of the solute concentration using: (a) the basic scheme; and (b) including condition (72) after any number of time steps.

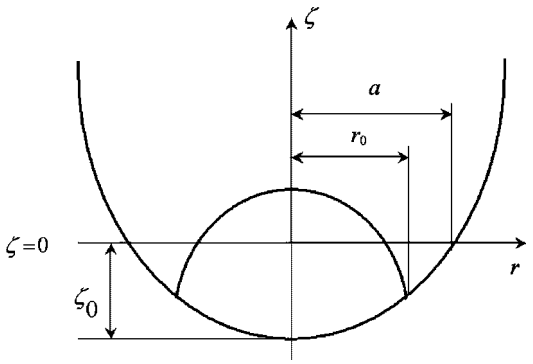

Figure 9. Initial free surface and water depth profile for the parabolic basin test.

concentration distribution functions are given by

$$z(x,y)=\begin{cases}100, & -100\leqslant x\leqslant 100,\ -100\leqslant y\leqslant 100\\ 0 & \text{otherwise}\end{cases} \tag{85}$$

$$h(x,y)=\begin{cases}0, & -100\leqslant x\leqslant 100,\ -100\leqslant y\leqslant 100\\ 1 & \text{otherwise}\end{cases} \tag{86}$$

$$\phi(x,y)=\begin{cases}0, & -100\leqslant x\leqslant 100,\ -100\leqslant y\leqslant 100\\ 100 & \text{otherwise}\end{cases} \tag{87}$$

The same mesh used of the previous test case is applied in this case. Figure 8(a) shows a 3D view of water depth function and a contour plot of the solute concentration using the basic scheme after one time step. It can be observed how the initial constant water depth and solute

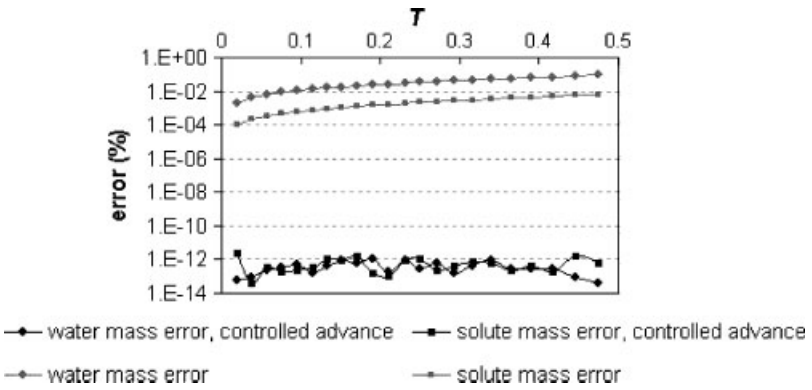

Figure 10. Water and solute mass error during wave expansion controlling wetting/drying advance and using the basic method.

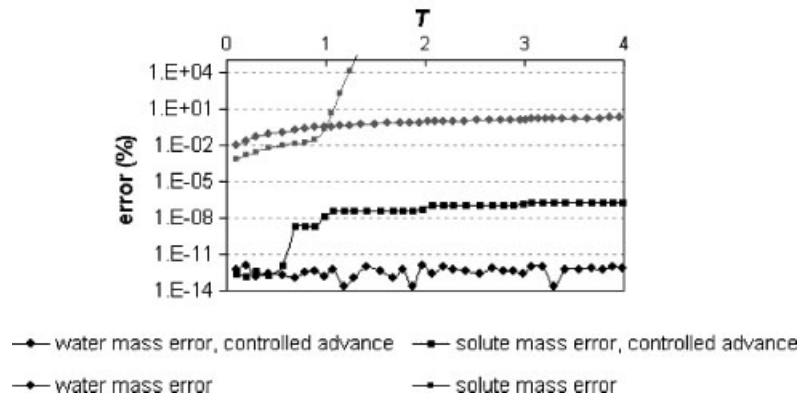

Figure 11. Water and solute mass error during wave expansion controlling wetting/drying advance and using the basic method.

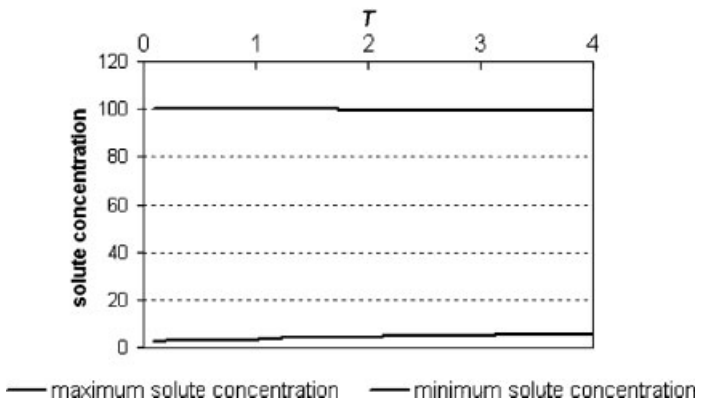

Figure 12. Maximum and minimum solute concentration along the simulation.

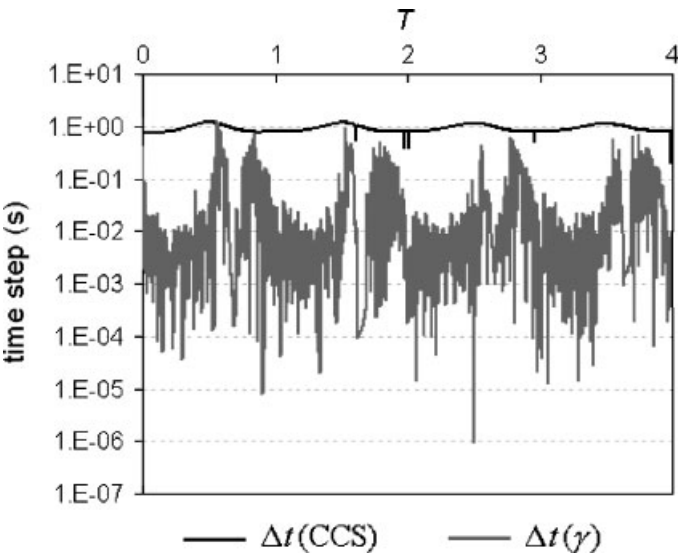

Figure 13. Simulation time step size with CCS and with condition (70).

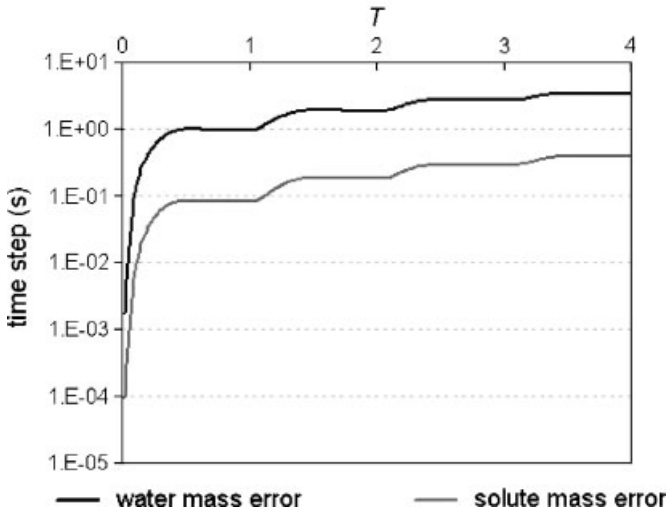

Figure 14. Mass conservation error when no entropy correction is used and following condition (26).

concentration are distorted. When condition (72) is applied, the initial solution is conserved, for both water depth and solute concentration at any later time, as Figure 8(b) shows.

Long wave resonance in a parabolic basin

The analytical solution of a long wave, driven by gravity and resonating in a frictionless, dry circular parabolic basin was presented by Thacker [33] for the shallow-water equations, where

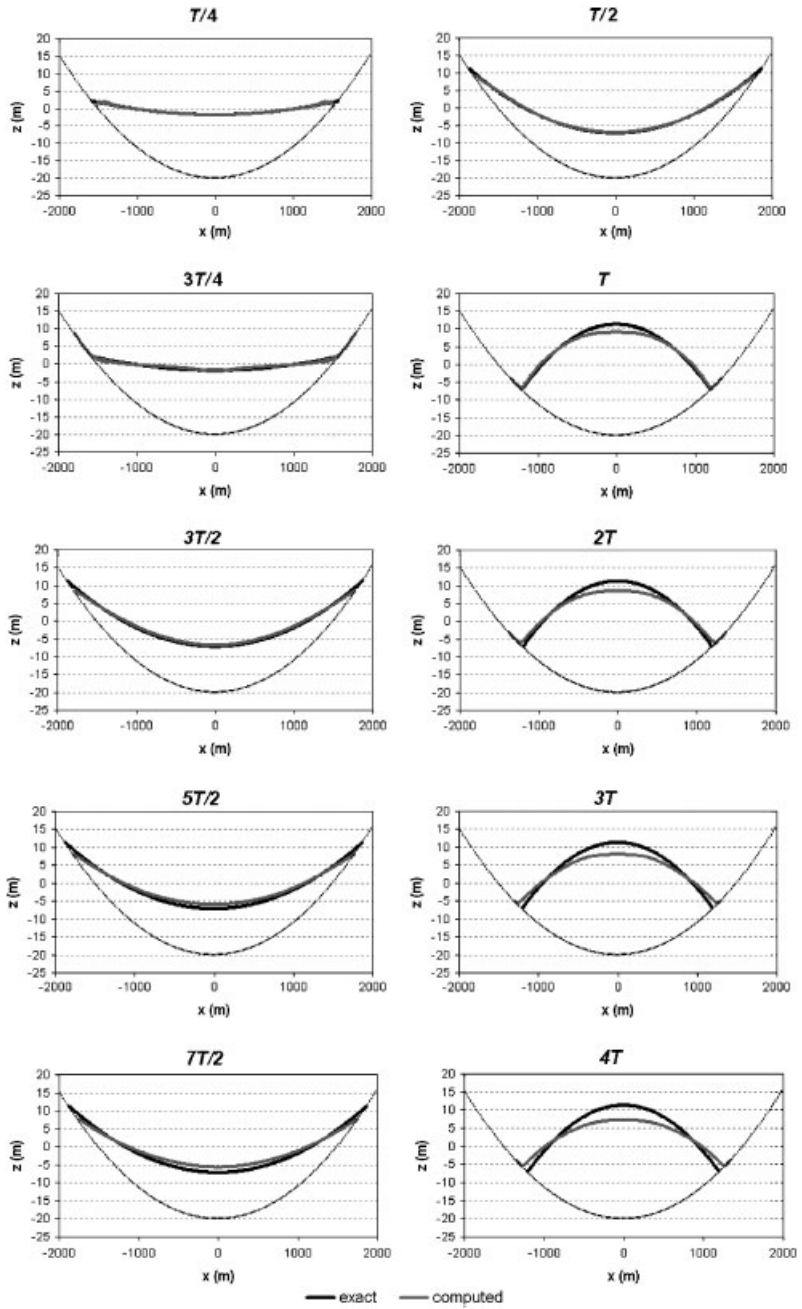

Figure 15. Water elevation surface (in metres): exact and simulated for times $1/4T$, $2/4T$, $3/4T$, T, $3/2T$, $2T$, $5/2T$, $3T$, $7T/2$ and $4T$.

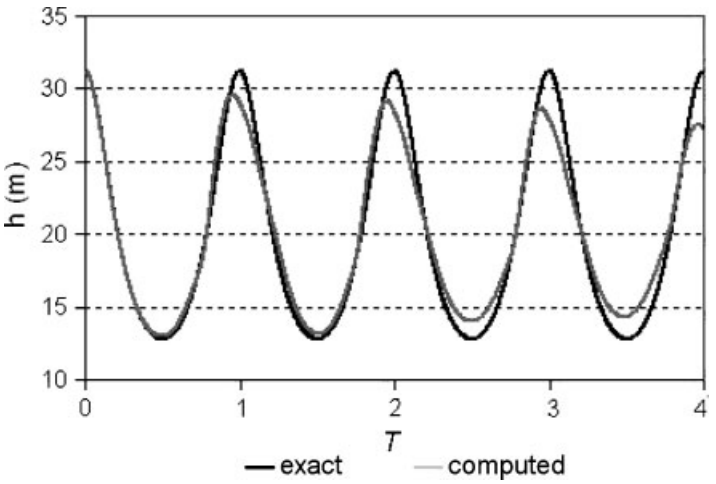

Figure 16. Water depth at the central point, exact and computed with CCS at $r = 0$.

the free surface displacement is given by

$$\zeta(r,t) = \zeta_o \left(\frac{(1-A^2)^{1/2}}{1 - A\cos\omega t} - 1 - \frac{r^2}{a^2} \left\{ \frac{1-A^2}{(1 - A\cos\omega t)^2} - 1 \right\} \right) \tag{88}$$

and the bottom elevation is given as

$$z(r,t) = -\zeta_0 \left(1 - \frac{r^2}{a^2} \right) \tag{89}$$

with

$$A = \frac{a^4 - r_o^4}{a^4 + r_o^4}, \quad \omega = \frac{1}{a}\sqrt{8g\zeta_o} \tag{90}$$

ζ_o is the centre point water depth, r is the distance from the centre point, a is the radial distance from the centre point to the zero elevation on the shoreline and r_o is the distance from the centre point to the point where the water depth is initially nil. Those values are represented in Figure 9. The domain shape of the two previous examples is used again and the numerical values are $\zeta_o = 20.0\,\text{m}$, $r_o = 1200\,\text{m}$, $a = 1500\,\text{m}$. The domain is divided in triangular cells with $l = 25\,\text{m}$ generated as in the previous sections.

The water surface movement will be simulated together with an initial solute concentration:

$$\phi(r,t_o) = \phi_o \exp\left(-\frac{r}{2r_o} \right) \tag{91}$$

There is no analytical solution for the solute concentration evolution in time but, if no diffusion is assumed, the solution for each T oscillation period will be

$$\phi(r, t = TK) = \phi_o \exp\left(-\frac{r}{2r_o} \right), \quad K = 1, \ldots, \infty \tag{92}$$

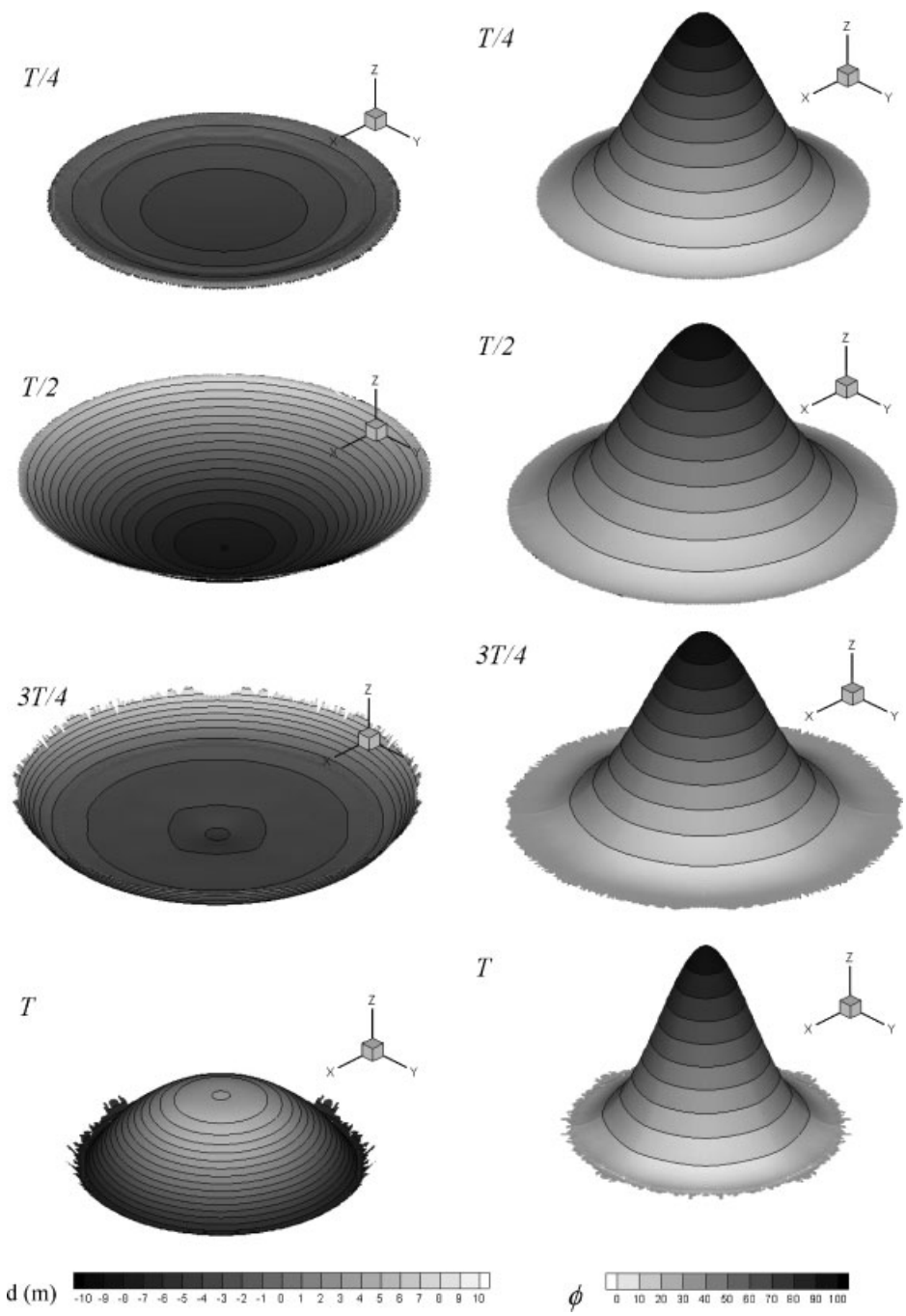

Figure 17. 3D view for the water level surface (left side) and 3D view of the solute concentration (right side) computed at times $1/4T$, $2/4T$, $3/4T$ and T.

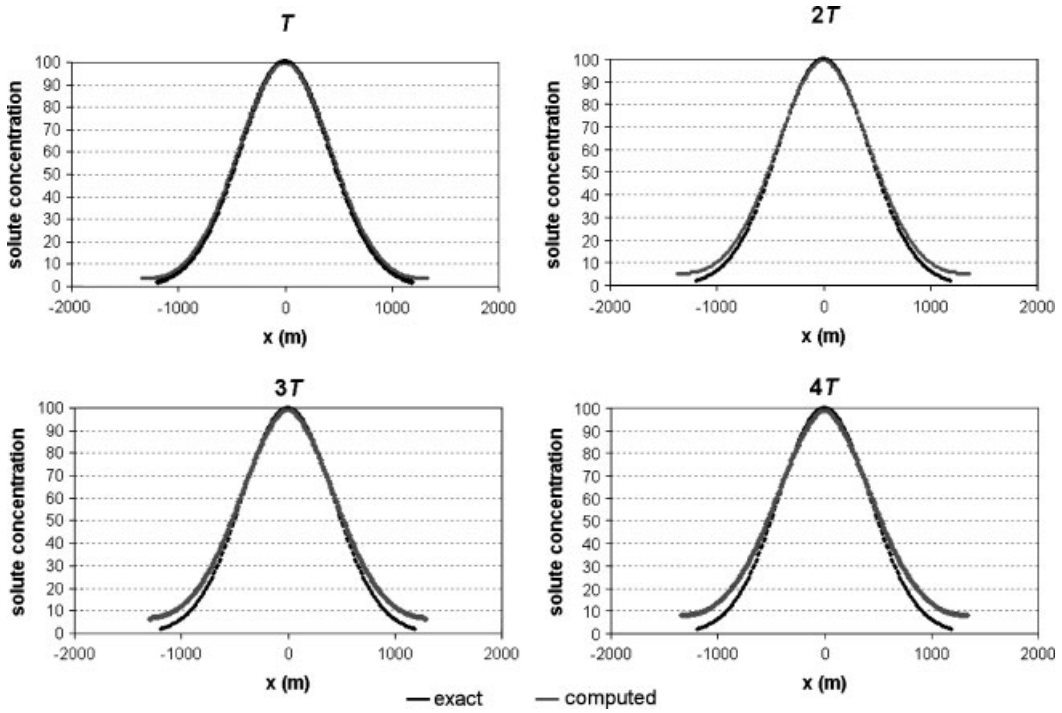

Figure 18. Solute distribution results and exact solution at times T, $2T$, $3T$ and $4T$.

The numerical experiment is performed using $\phi_o = 1$. This test case illustrates the concepts described in this paper, as it includes wetting/drying fronts and the generation of dry regions from wet areas. In particular, the advance of the wetting/drying front is produced in the first half period, during the wave expansion, while during the wave contraction both wetting/drying fronts and drying process are present. Figure 10 shows the water and solute mass conservation errors versus time during the wave expansion using the proposed method, and neglecting condition (72), that is considering nil the values of water depth and solute mass if they become negative. Only considering (72), positivity is guaranteed for both water and solute mass ensuring conservation at the same time.

Figure 11 displays the water and solute mass errors if the simulation progresses until $t = 4T$ using CCS and using the basic method that puts to zero the values of water depth and solute mass if negative. In this case, the proposed method conserves mass during all the simulation. If no special techniques are applied in the wetting advance or in the drying processes, the water mass error grows continuously and, after a short time, the solute mass error goes out of range.

Figure 12 shows both maximum and minimum solute concentration values as a function of the periods covered by the simulation, and how almost no numerical diffusion is produced. Figure 13 provides the simulation time steps used by the proposed CCS and by means of a more restrictive condition in (70), showing important differences in the magnitude. The fluctuating values in the time step size when using condition (70) are a consequence of

Table I. Maximum and minimum water depth elevations and concentrations at times $1/4T$, $2/4T$, $3/4T$ and T.

Time	Max d (m)	Min d (m)	Max ϕ	Min ϕ
$1/4T$	1.618	−1.864	99.961	2.927
$2/4T$	8.576	−7.008	99.961	3.286
$3/4T$	8.536	−2.123	99.930	3.294
T	9.019	−6.576	99.834	3.298

the presence of drying cells. Although they do not affect the accuracy of the solution, they significantly influence the efficiency of the algorithm. Figure 14 displays the mass conservation error generated when no entropy correction is done over the source terms following condition (26), leading to a continuous growth of this function.

Figure 15 shows the water depths given by the exact solution and by the proposed method at times, $1/4T$, $2/4T$, $3/4T$, T, $3/2T$, $2T$, $5/2T$, $3T$, $7T/2$ and $4T$. The simulated results prove in every case in good agreement with the analytical solution, including water depth and inundated area, even in the fourth oscillation. Figure 16 displays the water depth at the central point, $r = 0$, as function of the oscillation period, T. The computed solution deviates from the analytical solution as time increases, but the error grows slowly. Figure 17 displays 3D views for the water level surface and for the solute concentration computed at times $1/4T$, $2/4T$, $3/4T$ and T, and how the symmetry of the problem is kept along the simulation. Figure 18 shows the comparison between the exact and numerical solution for the solute concentration distribution at times T, $2T$, $3T$ and $4T$. Better accuracy in the final solution can be achieved by reducing the size of the cells generating a better representation of the bottom elevation (Table I).

APPLICATION: TOCE RIVER TEST CASE

The Toce river is a watercourse of the occidental Alps, in Italy. A scaled physical model was built at the ENEL laboratory in Milan with a horizontal scale factor of 1:100 and approximate dimensions of 50×11 m. The model reproduces a reach of the riverbed, the floodplain, a lateral reservoir designed for flood control purposes and buildings. The friction was modelled using $n = 0.0162\,\mathrm{s\,m^{-1/3}}$. Moreover the model reproduces details of the geometry. On the upstream side of the model, a tank was installed to supply the inflow of water in the form of a discharge hydrograph, characterized by a sharp peak shown in Figure 19.

The bed valley was initially dry and the subsequent flood wave produced the overtopping of the reservoir. Several water depth probes were situated in different places along the river bed and in the valley, as Figure 20 displays.

In this case, the flooding presents various transitions from subcritical to supercritical, and the wetting/drying techniques presented have to cope with high variable bed regions, specially in a initially dry reservoir, which is overtopped. Figure 21 shows good agreement between measured and computed data in the probes located at different points along the domain.

In this example, the mesh has been adapted to the contour of the buildings represented in the laboratory model as cubes, to prove that the method copes correctly with high slopes.

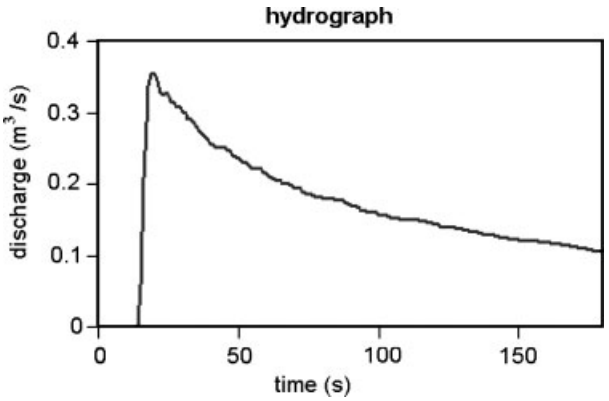

Figure 19. Discharge hydrograph. Toce river test case.

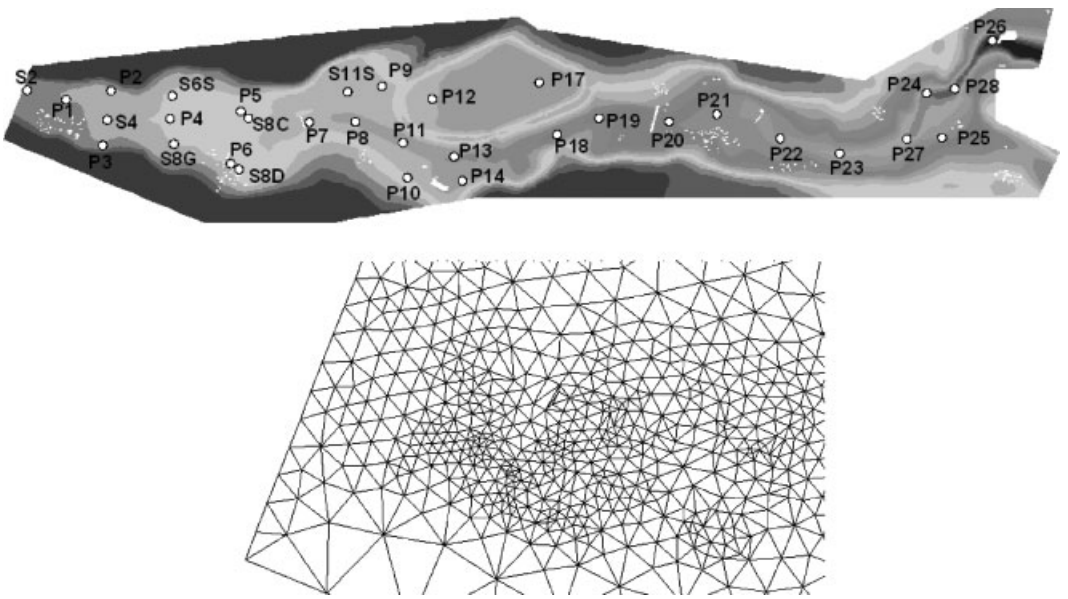

Figure 20. Toce river geometry and location of probes (upper) and detail of the mesh in the inlet region (lower) with 29 596 cells.

After the peak discharge, the discharge begins to decrease, and the buildings located close to the inlet boundary are high enough not to be overtopped. When the conditions discussed for wetting/drying cases are not applied, the method itself cannot manage these cases correctly. Figure 22 shows the results at time 180 s when the method is applied to the Toce flooding, using condition (57) for the time step. The left side of the figure corresponds to the application

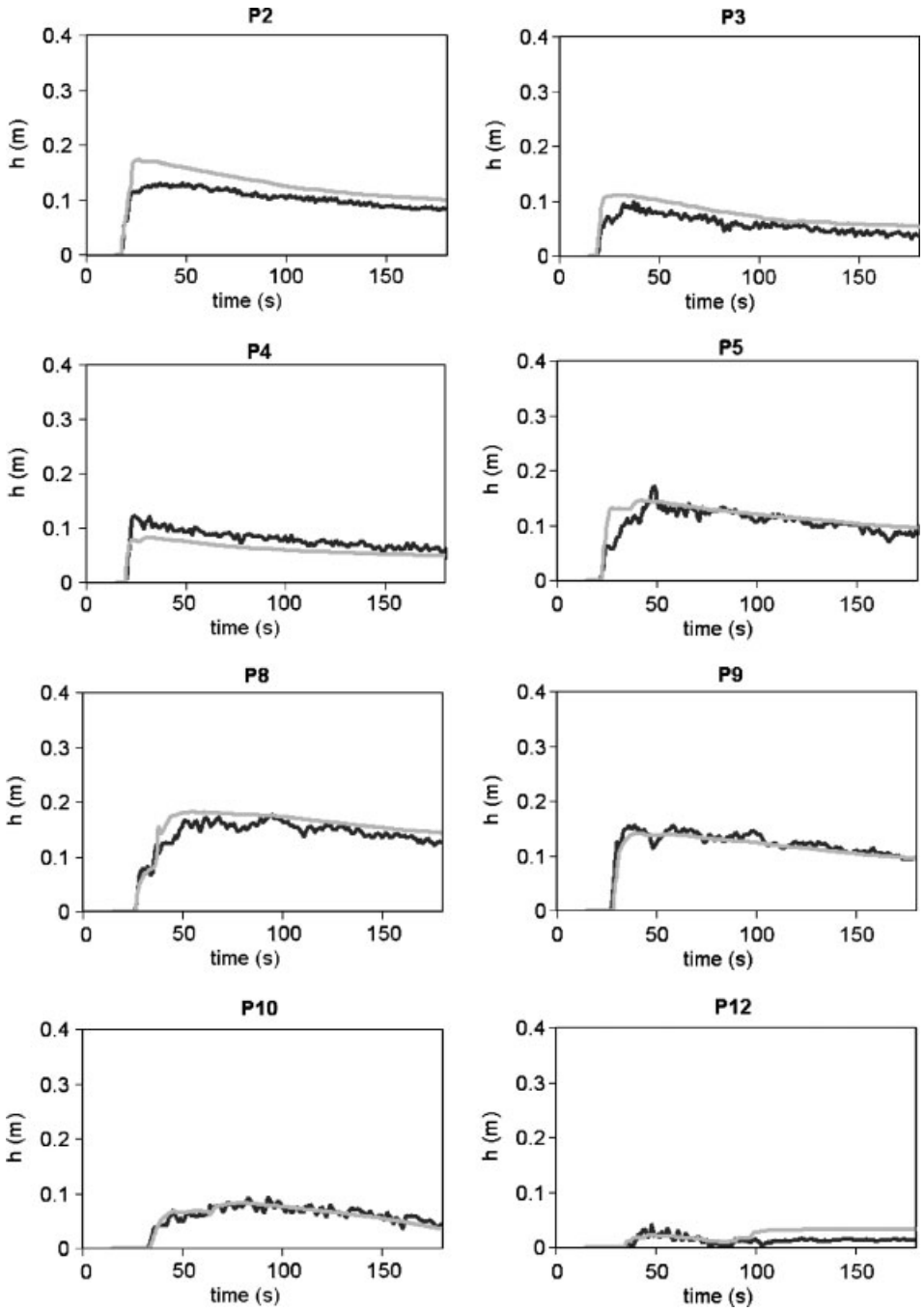

Figure 21. Comparison between numerical and measured data for different probes.

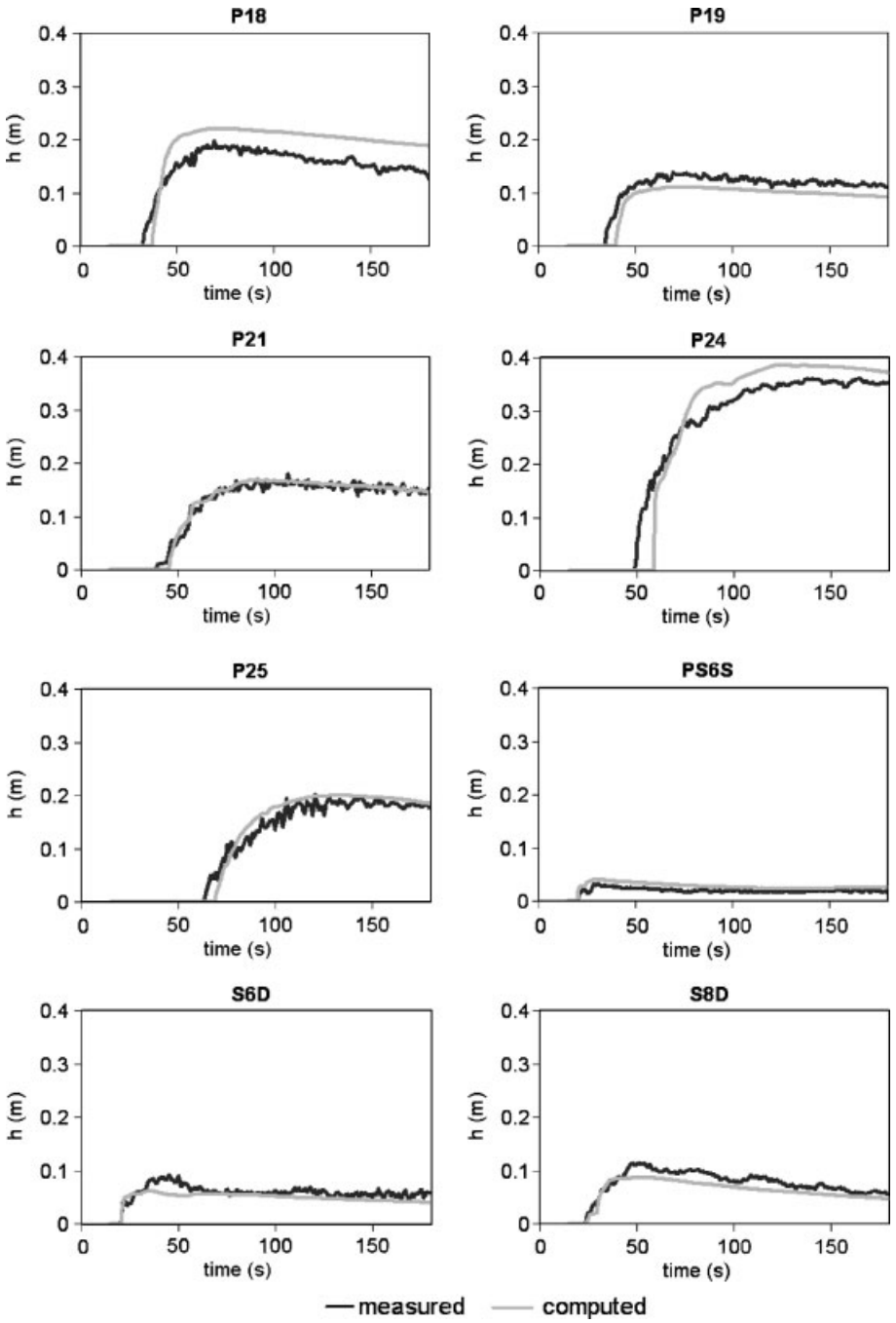

Figure 21. *Continued.*

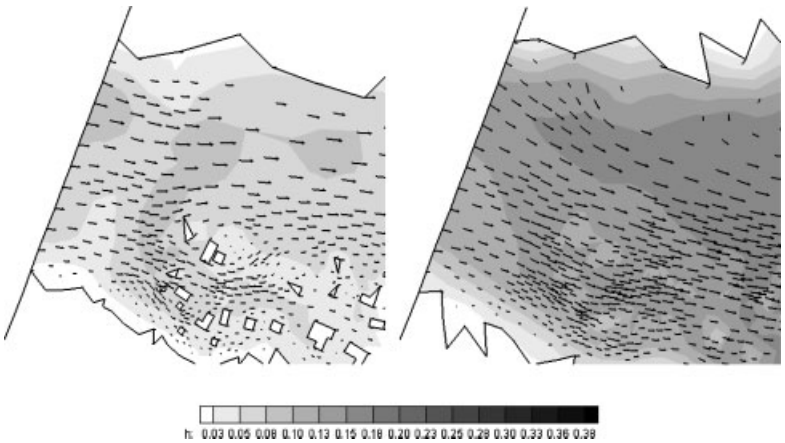

Figure 22. Values of water depth (in metres) at time 180 s, using CCS (left), and only making null negative values of depth (right).

of CCS and the right side to the strategy of making nil the negative values of depth if they appear. Not only the mass error is unacceptable, but also the buildings are overtopped.

No solute concentrations were measured in this test case. However, we have simulated the sudden release of a certain amount of solute as the flooding wave progresses, exactly at $t = 20$ s, at the location shown in Figure 23(a). The evolution of the solute concentration distribution at times $t = 23$, 26 and 30 s are displayed in Figure 23(b), (c) and (d), respectively.

Although no experimental data are available to state the accuracy of the solute transport in this case, the solution is well behaved and remains conservative in water mass as well as solute mass as time progresses. In absence of diffusion, the purely advective transport relies on the quality of the velocity field. It is important to stress, however, that good quality experimental data are in progress in order to validate this method in complex cases of unsteady flow with transport.

CONCLUSIONS

An explicit upwind scheme has been used to solve a 2D coupled shallow-water/solute transport system of equations in complex situations. The formulation follows a conservative form where the updated variables are water depth, unit depth-averaged discharges and solute mass per unit area. The finite volume numerical technique has been designed to deal with both triangular or quadrilateral grids from an unstructured point of view. The transfer of information between cells has been formulated according to an algorithm based on cell interfaces and following a wave propagation point of view much closer to the physical meaning of the equations than the usual numerical flux. The upwind discretization has been applied to the coupled scheme in a compact form that unifies the treatment of flux derivatives and bed slope source terms by means of a redefinition of the advection velocities.

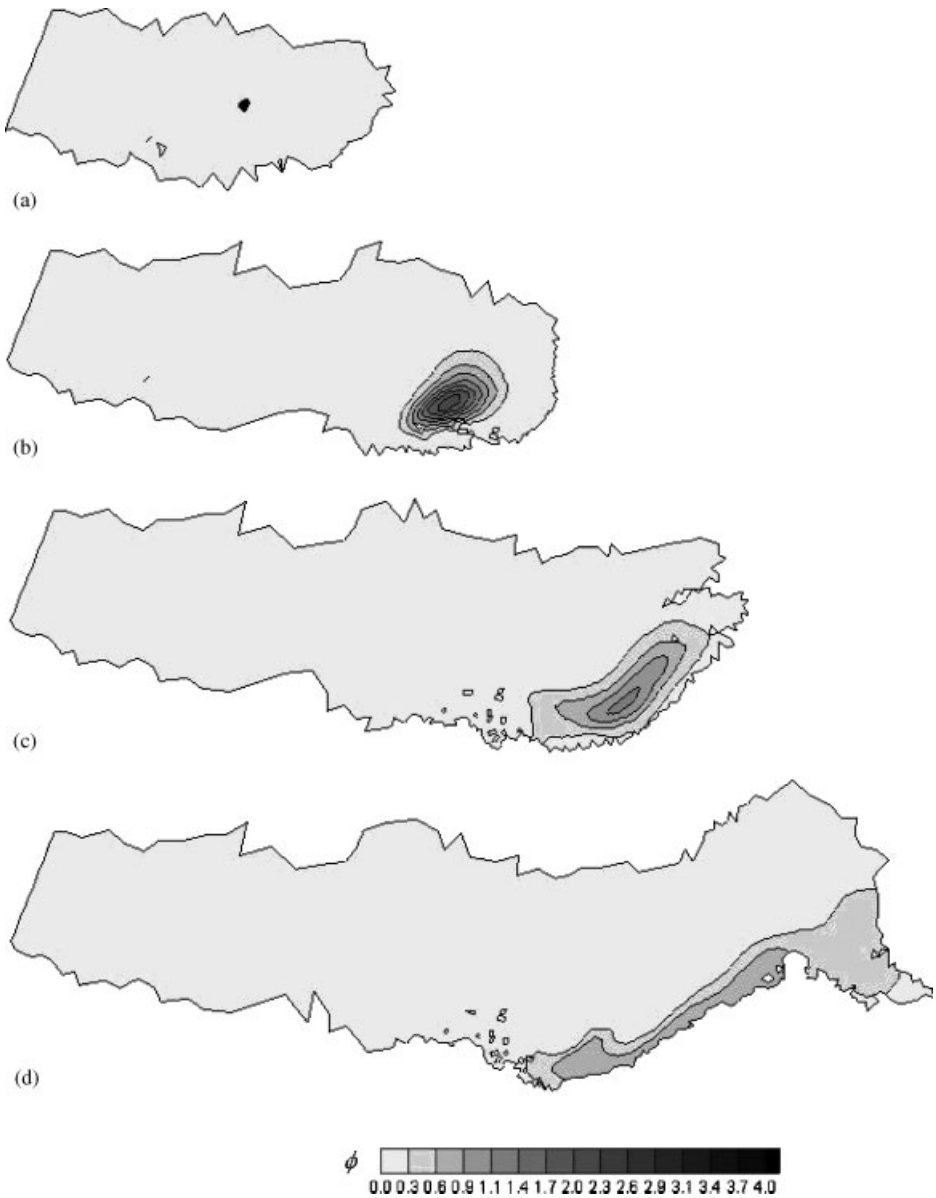

Figure 23. Evolution of an instantaneous injection of solute at time: (a) 20 s, and evolution at times (b) 23; (c) 26; and (d) 30 s.

These ideas have been helpful in the analysis of the numerical stability constraints. Starting by the simplest scalar homogeneous case, the stability constraints have been revisited and the basic CFL condition has been first properly stated for triangular and quadrilateral grids in the basic case and replaced by a stronger condition linked to the bed variations and the transient

character of the flow over a dry bed. The presence of these flow features imposes a heavier restriction on the time step size that can lead to very inefficient computations. A technique to avoid the necessity of reducing the time step that, at the same time, prevents instability and ensures conservation at all times has been proposed.

On the other hand, it has been realized that the solute transport advancing fronts in the shallow-water body require special numerical treatment in some cases, particularly when the solute concentration discontinuity is located at the same place of a water-depth discontinuity. Although the numerical solutions for the conserved variables supplied by the numerical scheme are always monotone, this is not the case for the solute concentration. An efficient way to avoid unbounded values of solute concentration within the framework of the scheme has been presented.

Numerical techniques developed in the last decade to solve realistic problems do not always face properly source term discretization, treatment of wetting–drying fronts or the specific numerical stability restrictions. This work completes the requirements on a first-order upwind conservative scheme to be used with success in Hydraulic Engineering.

ACKNOWLEDGEMENTS

This work was funded in part by the Spanish Ministry of Science and Technology under project PETRI. Additional support was provided by the European Research project IMPACT.

REFERENCES

1. Cunge JA, Holly FM, Verwey A. *Practical Aspects of Computational River Hydraulics*. Pitman: London, U.K., 1980.
2. Bellos CV, Soulis JV, Sakkas JG. Computation of two-dimensional dam-break induced flows. *Advances in Water Research* 1991; **14**(1):31–41.
3. Alcrudo F, García-Navarro P. A high resolution Godunov-type scheme in finite volumes for the 2D shallow water equations. *International Journal for Numerical Methods and Fluids* 1993; **16**(6):489–505.
4. Sleigh PA, Berzins M, Gaskell PH, Wright NG. An unstructured finite volume algorithm for predicting flow in rivers and stuaries. *Computers and Fluids* 1998; **27**(4):479–508.
5. Bermúdez A, Dervieux A, Desideri JA, Vázquez ME. Upwind schemes for the two-dimensional shallow water equations with variable depth using unstructured meshes. *Computers and Methods in Applied Mechanical Engineering* 1998; **155**:49–72.
6. García-Navarro P, Vázquez-Cendón ME. On numerical treatment of the source terms in the shallow water equations. *Computers and Fluids* 2000; **29**:951–979.
7. Zhao DH, Shen HW, Tabios GQ, Lai JS, Tan WY. Finite volume two-dimensional unsteady flow model for river basins. *Journal of Hydraulic Engineering* 1994; **120**(7):863–883.
8. Akanbi AA, Katopodes ND. Model for flood propagation on initially dry land. *Journal of Hydraulic Engineering* 1987; **114**(7):689–706.
9. Meshelle EA, Holly FM. Simulation of unsteady flow in irrigation canals with a dry bed. *Journal of Hydraulic Engineering* (ASCE) 1993; **119**:1021–1030.
10. Tchamen GW, Kahawita R. The numerical simulation of wetting and drying areas using Riemann solvers. *Proceedings of Modelling of Flood Propagation over Initially Dry Areas*, Milan, Italy, 1994.
11. Kramer A, Jozsa J, Sarkkula J. Hydrodynamic modeling aspects in the restoration planning of a coastal wetland. *Proceedings of the XXIX IAHR Congress*, Beijing, 2001.
12. Beffa C, Connel R. Two-dimensional flood plain flow. I: Model description. *Journal of Hydraulic Engineering* 2001; **6**(5):397–405.
13. George KJ, Stripling S. Improving the simulation of drying and wetting in a two-dimensional tidal numerical model. *Applied Mathematical Modeling* 1995; **19**(1):2–6.
14. Heniche M, Secretan Y, Boudreau P, Leclerc M. A two-dimensional finite element drying–wetting shallow water model for rivers and estuaries. *Advances in Water Research* 2000; **23**:359–372.
15. Kawahara M, Umetsu T. Finite element method for moving boundary problems in river flow. *International Journal for Numerical Methods in Fluids* 1986; **6**:365–386.

16. Khan AA. Modeling flow over an initially dry bed. *Journal of Hydraulic Research* 2000; **38**(5):383–389.
17. Bradford SF, Sanders BF. Finite-volume model for shallow water flooding of arbitrary topography. *Journal of Hydraulic Engineering* 2002; **128**(3):289–298.
18. Brufau P, Vázquez-Cendón ME, García-Navarro P. A numerical model for the flooding and drying of irregular domains. *International Journal for Numerical Methods in Fluids* 2002; **39**:247–275.
19. Brufau P, García-Navarro P, Vázquez-Cendón ME. Zero mass error using unsteady wetting/drying conditions in shallow flows over dry irregular topography. *International Journal for Numerical Methods in Fluids* 2004; **45**:1047–1082.
20. Vázquez-Cendón ME. Improved treatment of source terms in upwind schemes for the shallow water equations in channels with irregular geometry. *Journal of Computational Physics* 1999; **148**:497–526.
21. Abbot MB. *Computational Hydraulics*. Ashgate Publication Company: New York, 1992.
22. Holly FM. Two dimensional mass dispersion in rivers. *Hydro*. *Paper No*., 78, Colorado State University, Fort Collins, Colo. 1975.
23. Murillo J, Burguete J, Brufau P, García-Navarro P. Coupling between shallow water and solute flow equations: analysis and management of source terms in 2D. *International Journal for Numerical Methods in Fluids* 2005; **49**:267–299.
24. Godlewsky E, Raviart PA. *Numerical Approximation of Hyperbolic Systems of Conservation Laws*. Springer: Berlin, 1996.
25. Roe PL. Discrete models for the numerical analysis of time dependent multidimensional gas dynamics. *Journal of Computational Physics* 1986; **63**:458–476.
26. LeVeque RJ. Balancing source terms and flux gradients in high-resolution Godunov methods: the quasi-steady wave-propagation algorithm. *Journal of Computational Physics* 1998; **146**(1):346–365.
27. Hubbard ME, García-Navarro P. Flux difference splitting and the balancing of source terms and flux gradients. *Journal of Computational Physics* 2000; **165**:89–125.
28. Bermúdez A, Vázquez ME. Upwind methods for hyperbolic conservation laws with source terms. *Computers and Fluids* 1998; **8**:1049–1071.
29. Harten A, Hyman JM. Self adjusting grid methods for one-dimensional hyperbolic conservation laws. *Journal of Computational Physics* 1983; **50**:235–269.
30. Hirsch C. *Numerical Computation of Internal and External Flows*, vol. 2. Wiley: New York, 1990.
31. Murillo J, García-Navarro P, Brufau P, Burguete J. Extension of an explicit finite volume method to large time steps (CFL $>$ 1): application to shallow water flows. *International Journal for Numerical Methods in Fluids* 2006; **50**:63–102.
32. Courant R, Isaacson E, Reeves M. On the solution of non-linear hyperbolic conservation laws. *Communication on Pure and Applied Mathematics* 1952; **5**:243–255.
33. Thacker WC. Some exact solutions to the nonlinear shallow water equations. *Journal of Fluid Mechanics* 1981; **107**:499–508.

